NUREG/CR-5327
MEA-2265

Slow Strain Rate Testing of a Cyclically Stabilized A 516 Gr. 70 Piping Steel in PWR Conditions

Prepared by H. E. Hanninen, W. H. Cullen

Materials Engineering Associates, Inc.

Prepared for
U.S. Nuclear Regulatory Commission

MASTER

DISTRIBUTION OF THIS DOCUMENT IS UNLIMITED

AVAILABILITY NOTICE

Availability of Reference Materials Cited in NRC Publications

Most documents cited in NRC publications will be available from one of the following sources:

1. The NRC Public Document Room, 2120 L Street, NW, Lower Level, Washington, DC 20555

2. The Superintendent of Documents, U.S. Government Printing Office, P.O. Box 37082, Washington, DC 20013-7082

3. The National Technical Information Service, Springfield, VA 22161

Although the listing that follows represents the majority of documents cited in NRC publications, it is not intended to be exhaustive.

Referenced documents available for inspection and copying for a fee from the NRC Public Document Room include NRC correspondence and internal NRC memoranda; NRC Office of Inspection and Enforcement bulletins, circulars, information notices, inspection and investigation notices; Licensee Event Reports; vendor reports and correspondence; Commission papers; and applicant and licensee documents and correspondence.

The following documents in the NUREG series are available for purchase from the GPO Sales Program: formal NRC staff and contractor reports, NRC-sponsored conference proceedings, and NRC booklets and brochures. Also available are Regulatory Guides, NRC regulations in the *Code of Federal Regulations*, and *Nuclear Regulatory Commission Issuances*.

Documents available from the National Technical Information Service include NUREG series reports and technical reports prepared by other federal agencies and reports prepared by the Atomic Energy Commission, forerunner agency to the Nuclear Regulatory Commission.

Documents available from public and special technical libraries include all open literature items, such as books, journal and periodical articles, and transactions. *Federal Register* notices, federal and state legislation, and congressional reports can usually be obtained from these libraries.

Documents such as theses, dissertations, foreign reports and translations, and non-NRC conference proceedings are available for purchase from the organization sponsoring the publication cited.

Single copies of NRC draft reports are available free, to the extent of supply, upon written request to the Office of Information Resources Management, Distribution Section, U.S. Nuclear Regulatory Commission, Washington, DC 20555.

Copies of industry codes and standards used in a substantive manner in the NRC regulatory process are maintained at the NRC Library, 7920 Norfolk Avenue, Bethesda, Maryland, and are available there for reference use by the public. Codes and standards are usually copyrighted and may be purchased from the originating organization or, if they are American National Standards, from the American National Standards Institute, 1430 Broadway, New York, NY 10018.

DISCLAIMER NOTICE

This report was prepared as an account of work sponsored by an agency of the United States Government. Neither the United States Government nor any agency thereof, or any of their employees, makes any warranty, expresed or implied, or assumes any legal liability of responsibility for any third party's use, or the results of such use, of any information, apparatus, product or process disclosed in this report, or represents that its use by such third party would not infringe privately owned rights.

DISCLAIMER

This report was prepared as an account of work sponsored by an agency of the United States Government. Neither the United States Government nor any agency thereof, nor any of their employees, makes any warranty, express or implied, or assumes any legal liability or responsibility for the accuracy, completeness, or usefulness of any information, apparatus, product, or process disclosed, or represents that its use would not infringe privately owned rights. Reference herein to any specific commercial product, process, or service by trade name, trademark, manufacturer, or otherwise does not necessarily constitute or imply its endorsement, recommendation, or favoring by the United States Government or any agency thereof. The views and opinions of authors expressed herein do not necessarily state or reflect those of the United States Government or any agency thereof.

DISCLAIMER

Portions of this document may be illegible in electronic image products. Images are produced from the best available original document.

NUREG/CR--5327

TI90 002601

Slow Strain Rate Testing of a Cyclically Stabilized A 516 Gr. 70 Piping Steel in PWR Conditions

Manuscript Completed: October 1989
Date Published: November 1989

Prepared by
H. E. Hanninen,* W. H. Cullen

Materials Engineering Associates, Inc.
9700-B Martin Luther King, Jr. Highway
Lanham, MD 20706-1837

*Visiting Scientist from
Technical Research Centre of Finland (VTT)
Metals Laboratory
Kemistintie 3
02150 Espoo 15, Finland

MASTER

Prepared for
Division of Engineering
Office of Nuclear Regulatory Research
U.S. Nuclear Regulatory Commission
Washington, DC 20555
NRC FIN B8900

DISTRIBUTION OF THIS DOCUMENT IS UNLIMITED

ABSTRACT

In fatigue, both monotonic and cyclic plastic zones are formed ahead of the crack tip, inside which the strain history can be studied on the basis of stable hysteresis loops and their development. A 516 Gr. 70 piping steel was prefatigued to represent the material structure anticipated in the process zone and in the area of the maximum tensile stress ahead of the crack-tip. With these materials, slow strain rate tests were performed both in bulk PWR-environments and in the simulated crack-tip environments (MnS-contaminated water). Environment-sensitive cracking occurred in the simulated crack tip environments and in tests where external polarization was used to polarize the specimens to 0.0 mV(SHE) in both the MnS-contaminated and pure PWR-water. No marked difference was observed between as-received material and prefatigued materials. Usually the residual hydrogen content of the gage length section was increased after SSRT-testing, but based on the limited number of tests no clear conclusions could be drawn.

CONTENTS

		Page
ABSTRACT		iii
LIST OF FIGURES		vi
LIST OF TABLES		vii
FOREWORD		ix
ACKNOWLEDGMENT		xv
1.	INTRODUCTION	1
2.	WORKING HYPOTHESIS	3
3.	EXPERIMENTAL METHODS	5
	3.1 Test Material	5
	3.2 Cyclic Prestraining	7
	3.3 SSRT-Specimen Preparation	7
	3.4 SSRT-Testing Conditions	7
	3.5 Analysis of the Test Results	10
4.	RESULTS	12
	4.1 Cyclic Prestraining	12
	4.2 Microstructures	12
	4.3 Slow Strain Rate Tests	24
	4.4 Residual Hydrogen Contents	39
5.	DISCUSSION	41
6.	CONCLUSIONS	43
REFERENCES		44

LIST OF FIGURES

Figure		Page
1	Cutting diagram for A 516 Gr. 70 pipe	6
2	Specimen used to prestrain the piping steel	8
3	Slow strain rate test specimen	8
4	Schematic of the autoclave	9
5	Cyclic stress-strain curves of A 516 Gr. 70 steel	13
6	Optical microstructures of A 516 Gr. 70 steel	15
7	Transmission electron microscopy microstructures	18
8	Fracture surfaces from pure water tests	26
9	Fracture surfaces from PWR-water tests	27
10	Fracture surface from MnS-saturated PWR Water tests	28
11	Fracture surfaces from free and controlled potential tests in PWR water	29
12	Fracture surfaces from free and controlled potential tests in MnS-Saturated water	30
13	Fracture surface of low strain specimen tested in MnS-saturated PWR water	31
14	Details of the fracture surface from Fig. 13	32
15	Fracture surfaces of low strain specimens under potential control	33
16	Fracture surfaces of high strain specimens	34
17	Fracture surface of high strain specimen tested in MnS-saturated PWR-Water	35
18	Fracture surface of high strain specimen tested in MnS-saturated PWR-Water under potential control	38

LIST OF TABLES

Table		Page
1.	Composition of A 516 Gr.70 Steel	5
2.	Properties of A 516 Gr. 70 Piping Steel	5
3.	Nominal Water Chemistry Specification	10
4.	Summary of the SSRT Test Results	25
5.	SCC Crack Growth Rates	37
6.	Residual Hydrogen Contents	40

FOREWORD

The work reported here was performed at Materials Engineering Associates (MEA) under the program, Structural Integrity of Water Reactor Pressure Boundary Components, F. J. Loss, Program Manager. The program is sponsored by the Office of Nuclear Regulatory Research of the U. S. Nuclear Regulatory Commission (NRC). The technical monitor for the NRC is Alfred Taboada.

Prior reports under the current contract are listed below:

1. J. R. Hawthorne, "Significance of Nickel and Copper Content to Radiation Sensitivity and Postirradiation Heat Treatment Recovery of Reactor Vessel Steels," USNRC Report NUREG/CR-2948, Nov. 1982.

2. "Structural Integrity of Water Reactor Pressure Boundary Components, Annual Report for 1982," F. J. Loss, Ed., USNRC Report NUREG/CR-3228, Vol. 1, Apr. 1983.

3. J. R. Hawthorne, "Exploratory Assessment of Postirradiation Heat Treatment Variables in Notch Ductility Recovery of A 533-B Steel," USNRC Report NUREG/CR-3229, Apr. 1983.

4. W. H. Cullen, K. Torronen, and M. Kemppainen, "Effects of Temperature on Fatigue Crack Growth of A 508-2 Steel in LWR Environment," USNRC Report NUREG/CR-3230, Apr. 1983.

5. "Proceedings of the International Atomic Energy Agency Specialists' Meeting on Subcritical Crack Growth," Vols. 1 and 2, W. H. Cullen, Ed., USNRC Conference Proceeding NUREG/CP-0044, May 1983.

6. W. H. Cullen, "Fatigue Crack Growth Rates of A 508-2 Steel in Pressurized, High-Temperature Water," USNRC Report NUREG/CR-3294, June 1983.

7. J. R. Hawthorne, B. H. Menke, and A. L. Hiser, "Light Water Reactor Pressure Vessel Surveillance Dosimetry Improvement Program: Notch Ductility and Fracture Toughness Degradation of A 302-B and A 533-B Reference Plates from PSF Simulated Surveillance and Through-Wall Irradiation Capsules," USNRC Report NUREG/CR-3295, Vol. 1, Apr. 1984.

8. J. R. Hawthorne and B. H. Menke, "Light Water Reactor Pressure Vessel Surveillance Dosimetry Improvement Program: Postirradiation Notch Ductility and Tensile Strength Determinations for PSF Simulated Surveillance and Through-Wall Specimen Capsules," USNRC Report NUREG/CR-3295, Vol. 2, Apr. 1984.

9. A. L. Hiser and F. J. Loss, "Alternative Procedures for J-R Curve Determination," USNRC Report NUREG/CR-3402, July 1983.

10. A. L. Hiser, F. J. Loss, and B. H. Menke, "J-R Curve Characterization of Irradiated Low Upper Shelf Welds," USNRC Report NUREG/CR-3506, Apr. 1984.

11. W. H. Cullen, R. E. Taylor, K. Torronen, and M. Kemppainen, "The Temperature Dependence of Fatigue Crack Growth Rates of A 351 CF8A Cast Stainless Steel in LWR Environment," USNRC Report NUREG/CR-3546, Apr. 1984.

12. "Structural Integrity of Light Water Reactor Pressure Boundary Components -- Four-Year Plan 1984-1988," F. J. Loss, Ed., USNRC Report NUREG/CR-3788, Sep. 1984.

13. W. H. Cullen and A. L. Hiser, "Behavior of Subcritical and Slow-Stable Crack Growth Following a Postirradiation Thermal Anneal Cycle," USNRC Report NUREG/CR-3833, Aug. 1984.

14. "Structural Integrity of Water Reactor Pressure Boundary Components: Annual Report for 1983," F. J. Loss, Ed., USNRC Report NUREG/CR-3228, Vol. 2, Sept. 1984.

15. W. H. Cullen, "Fatigue Crack Growth Rates of Low-Carbon and Stainless Piping Steels in PWR Environment," USNRC Report NUREG/CR-3945, Feb. 1985.

16. W. H. Cullen, M. Kemppainen, H. Hanninen, and K. Torronen, "The Effects of Sulfur Chemistry and Flow Rate on Fatigue Crack Growth Rates in LWR Environments," USNRC Report NUREG/CR-4121, Feb. 1985.

17. "Structural Integrity of Water Reactor Pressure Boundary Components: Annual Report for 1984," F. J. Loss, Ed., USNRC Report NUREG/CR-3228, Vol. 3, June 1985.

18. A. L. Hiser, "Correlation of C_v and K_{Ic}/K_{Jc} Transition Temperature Increases Due to Irradiation," USNRC Report NUREG/CR-4395, Nov. 1985.

19. W. H. Cullen, G. Gabetta, and H. Hanninen, "A Review of the Models and Mechanisms For Environmentally-Assisted Crack Growth of Pressure Vessel and Piping Steels in PWR Environments," USNRC Report NUREG/CR-4422, Dec. 1985.

20. "Proceedings of the Second International Atomic Energy Agency Specialists' Meeting on Subcritical Crack Growth," W. H. Cullen, Ed., USNRC Conference Proceeding NUREG/CP-0067, Vols. 1 and 2, Apr. 1986.

21. J. R. Hawthorne, "Exploratory Studies of Element Interactions and Composition Dependencies in Radiation Sensitivity Development," USNRC Report NUREG/CR-4437, Nov. 1985.

22. R. B. Stonesifer and E. F. Rybicki, "Development of Models for Warm Prestressing," USNRC Report NUREG/CR-4491, Jan. 1987.

23. E. F. Rybicki and R. B. Stonesifer, "Computational Model for Residual Stresses in a Clad Plate and Clad Fracture Specimens," USNRC Report NUREG/CR-4635, Oct. 1986.

24. D. E. McCabe, "Plan for Experimental Characterization of Vessel Steel After Irradiation," USNRC Report NUREG/CR-4636, Oct. 1986.

25. E. F. Rybicki, J. R. Shadley, and A. S. Sandhu, "Experimental Evaluation of Residual Stresses in a Weld Clad Plate and Clad Test Specimens," USNRC Report NUREG/CR-4646, Oct. 1986.

26. "Structural Integrity of Water Reactor Pressure Boundary Components: Annual Report for 1985," F. J. Loss, Ed., USNRC Report NUREG/CR-3228, Vol. 4, June 1986.

27. G. Gabetta and W. H. Cullen, "Application of a Two-Mechanism Model for Environmentally-Assisted Crack Growth," USNRC Report NUREG/CR-4723, Oct. 1986.

28. W. H. Cullen, "Fatigue Crack Growth Rates in Pressure Vessel and Piping Steels in LWR Environments," USNRC Report NUREG/CR-4724, Mar. 1987.

29. W. H. Cullen and M. R. Jolles, "Fatigue Crack Growth of Part-Through Cracks in Pressure Vessel and Piping Steels: Air Environment Results, USNRC Report NUREG/CR-4828, Oct. 1988.

30. D. E. McCabe, "Fracture Evaluation of Surface Cracks Embedded in Reactor Vessel Cladding: Unirradiated Bend Specimen Results," USNRC Report NUREG/CR-4841, May 1987.

31. H. Hanninen, M. Vulli, and W. H. Cullen, "Surface Spectroscopy of Pressure Vessel Steel Fatigue Fracture Surface Films Formed in PWR Environments," USNRC Report NUREG/CR-4863, July 1987.

32. A. L. Hiser and G. M. Callahan, "A User's Guide to the NRC's Piping Fracture Mechanics Data Base (PIFRAC)," USNRC Report NUREG/CR-4894, May 1987.

33. "Proceedings of the Second CSNI Workshop on Ductile Fracture Test Methods (Paris, France, April 17-19, 1985)," F. J. Loss, Ed., USNRC Conference Proceeding NUREG/CP-0064, Aug. 1988.

34. W. H. Cullen and D. Broek, "The Effects of Variable Amplitude Loading on A 533-B Steel in High-Temperature Air and Reactor Water Environments," USNRC Report NUREG/CR-4929, Apr. 1989.

35. "Structural Integrity of Water Reactor Pressure Boundary Components: Annual Report for 1986," F. J. Loss, Ed., USNRC Report NUREG/CR-3228, Vol. 5, July 1987.

36. F. Ebrahimi, et al., "Development of a Mechanistic Understanding of Radiation Embrittlement in Reactor Pressure Vessel Steels: Final Report," USNRC Report NUREG/CR-5063, Jan. 1988.

37. J. B. Terrell, "Fatigue Life Characterization of Smooth and Notched Piping Steel Specimens in 288°C Air Environments," USNRC Report NUREG/CR-5013, May 1988.

38. A. L. Hiser, "Tensile and J-R Curve Characterization of Thermally Aged Cast Stainless Steels," USNRC Report NUREG/CR-5024, Sept. 1988.

39. J. B. Terrell, "Fatigue Strength of Smooth and Notched Specimens of ASME SA 106-B Steel in PWR Environments," USNRC Report NUREG/CR-5136, Sept. 1988.

40. D. E. McCabe, "Fracture Evaluation of Surface Cracks Embedded in Reactor Vessel Cladding: Material Property Evaluations," USNRC Report NUREG/CR-5207, Sept. 1988.

41. J. R. Hawthorne and A. L. Hiser, "Experimental Assessments of Gundremmingen RPV Archive Material for Fluence Rate Effects Studies," USNRC Report NUREG/CR-5201, Oct. 1988.

42. J. B. Terrell, "Fatigue Strength of ASME SA 106-B Welded Steel Pipes in 288°C Air Environments," USNRC Report NUREG/CR-5195, Dec. 1988.

43. A. L. Hiser, "Post-Irradiation Fracture Toughness Characterization of Four Lab-Melt Plates," USNRC Report NUREG/CR-5216, Rev. 1, June 1989.

44. R. B. Stonesifer, E. F. Rybicki and D. E. McCabe, "Warm Prestress Modeling: Comparison of Models and Experimental Results," USNRC Report NUREG/CR-5208, Apr. 1989.

45. A. L. Hiser and J. B. Terrell, "Size Effects on J-R Curves for A 302-B Plate," USNRC Report NUREG/CR-5265, Jan. 1989.

46. D. E. McCabe, "Fracture Evaluation of Surface Cracks Embedded in Reactor Vessel Cladding," USNRC Report NUREG/CR-5326, Mar. 1989.

47. J. R. Hawthorne, "An Exploratory Study of Element Interactions and Composition Dependencies in Radiation Sensitivity Development: Final Report," USNRC Report NUREG/CR-5357, April 1989.

48. J. R. Hawthorne, "Steel Inpurity Element Effects on Postirradiation Properties Recovery by Annealing: Final Report," USNRC Report NUREG/CR-5388, August 1989.

ACKNOWLEDGMENT

The major experimental part of the work was carried out at Materials Engineering Associates, Inc. financed by NRC and the Technical Research Center of Finland. This program was managed by A. Taboada, the NRC Program Manager. The authors appreciate the SEM study performed by Mr. Markku Kemppainen and the TEM study carried out by Mr. Pertti Nenonen of Metallurgical Laboratory of the Technical Research Centre of Finland under Nuclear Materials Research Program financed by Ministry of Trade and Industry of Finland and Technical Research Centre of Finland.

1. INTRODUCTION

Reactor pressure vessel and piping carbon steels are known to crack in oxygenated high temperature pure water (BWR conditions) by a stress corrosion cracking (SCC) mechanism both in static (Ref. 1) and in dynamic SSRT tests (Refs. 2 to 11). Also, reactor pressure vessel steels are known to be susceptible to SCC in high-temperature, PWR primary side water if the corrosion potential is raised above -200 mV(SHE) by external potential control (Refs. 3, 12 to 14). Thus, there seems to be both in BWR and PWR water a critical potential for crack initiation at about -200 mV(SHE). However, there are indications in SSRT tests that, e.g., the MnS inclusions in the SSRT specimen surface debond from the matrix and form crevices inside which an aggressive environment is generated by dissolution of MnS. In these crevices, the minimum cracking potential can be lowered (for A 508-2 steel) to about -400 mV(SHE) (Ref. 2). Similarly, Klemetti and Hanninen, (Ref. 11), observed SCC in the ICCGR round robin test in which the corrosion potential was decreased from the susceptible SCC potential region into the anticipated safe region. Sulfate additions to high temperature water have produced a marked decrease in the critical potential for SCC of pressure vessel steels. (Ref. 15)

Phenomenologically, environment-sensitive cracking occurs in SSRT testing of reactor pressure vessel and piping steels in high temperature water with effects similar to the case of corrosion fatigue. Marked environmental enhancement can occur in corrosion fatigue of pressure vessel and piping steels in PWR primary water conditions where the corrosion potential is about -700 mV(SHE), which is much lower than the minimum stress corrosion cracking potential obtained in SSRT tests, about -200 mV(SHE).

Speidel and Magdowski, 1987 (Ref. 1), after summarizing the environment-sensitive crack growth data of pressure vessel steels in high temperature water, were able to conclude that sulfur content of the steel has no measurable effect on the stress corrosion crack growth rate and that there is no measurable indication of the effect of oxygen content or corrosion potential on growth rates of stress corrosion cracks. Only a small percentage of their fracture mechanics specimens indicated crack growth, suggesting it was important that the crack tip was initially located in a metallurgically inhomogeneous region. If so, it would be probable that this region was able to change the crack-tip conditions with respect to the bulk water, e.g., through dissolution of MnS sulfide particles as proposed by Hanninen et al. (Ref. 16), and Klemetti et al. (Ref. 17). Effects of dissolution of MnS particles on crevice chemistry have been also shown experimentally by using artifical crevices by Ford et al. (Ref. 18) and Illi et al., (Ref. 19); therefore: when the amount of aggressive species increases, the pH reduces, and conductivity increases. Klemetti and Hanninen (Ref. 11), and Hanninen et al. (Ref. 20) have shown that in simulated local crack-tip conditions, (i.e., saturated MnS solution), pressure vessel steels are susceptible to SCC even at very low corrosion potentials at 80°C. Also, the cracking susceptibility seems to correlate with the potential dependence of hydrogen absorption into the steel in hydrogen sulfide containing

environments. However, Congleton (Ref. 21) was able to show that in primary PWR-water no cracking was occurring and even the existing cracks were cathodically protected at -700 mV(SHE). These observations suggest that once the conditions for crack growth at the crack tip are obtained and can be sustained, cracking continues over a wide potential range. However, the initiation of cracking in bulk reactor water is only possible above the critical corrosion potential, where pitting corrosion at the MnS inclusions occurs and local sites for crack initiation are generated.

In corrosion fatigue crack growth, hydrogen sulfide has been proven to be the principal species responsible for observed enhancement of the fatigue crack growth rates in light water reactor conditions. Van Der Sluys and Emanuelson (Ref. 22) demonstrated this by injection of ppm levels of hydrogen sulfide into the corrosion fatigue crack tip of a low sulfur steel. Earlier it had been well established that the sulfur content of the pressure vessel steels is one of the major variables in determining the corrosion fatigue crack growth in LWR environments (Ref. 26, 23 to 26). Recently by using modern spectroscopic techniques it has been shown that sulfur which dissolves from MnS inclusions also stays inside the crack and is present in the corrosion product as iron sulfide (Ref. 27). Iron sulfide is also soluble in the crack-tip environment and can supply the hydrogen sulfide necessary to sustain enhanced crack growth, as happened in the case of Van Der Sluys and Emanuelson's experiment (Ref. 22), where high crack growth rate continued even after injection of hydrogen sulfide into the crack tip of low sulfur pressure vessel steel had ceased. In order to understand mechanistically the role of sulfur in corrosion fatigue crack growth, the effects of sulfur in both anodic dissolution and in hydrogen uptake has been studied and discussed (Refs. 28 to 32). Mechanistically, the problem is complex because the chemistry and electrochemistry inside the crack seem to favor both reactions (Ref. 28, 33-35).

2. WORKING HYPOTHESIS

Crack-tip strain and strain rate are the critical parameters affecting fatigue, corrosion fatigue, as well as stress corrosion crack growth rates. Estimates of crack-tip strain rates are generally performed under conditions of cyclically loaded long cracks in small scale yielding or monotonically loaded short cracks in large scale general yielding. Crack-tip strain rate has often been considered as the unifying parameter between corrosion fatigue (CF) and stress corrosion cracking (SCC) especially when slow strain rate testing technique (SSRT) is used as a link between the two. Crack-tip strain rate can also be used for correlating crack growth data obtained under different testing conditions. Fundamentally, if the strain rate at the growing crack tips of short SCC cracks in the SSRT specimens and of long CF cracks in the compact tension fracture mechanics specimens satisfies the required similitude, then similitude of the chemistry and electrochemistry inside the cracks of both types of tests must also be assured.

When the crack-tip strain rates from SSRT tests relating to short crack propagation in fully plastic material are correlated with the linear elastic fracture mechanics specimens used in corrosion fatigue testing, the cyclic strain history of the material ahead of the fatigue crack tip is not considered. Ahead of the corrosion fatigue crack tip, cyclic strain is occurring inside the cyclic plastic zone, which affects the metallurgical structure of this region by producing a cyclically stabilized deformation structure consisting of a dislocation cell structure, where the size of the cells corresponds to the amount of strain. Therefore, the flow properties inside this cyclic plastic zone are very different from the as-received materials typically used in SSRT tests. When the SSRT results are correlated with the CF data, this difference should be considered more carefully.

SSRT testing in normal PWR conditions has not produced SCC cracking, but often in CF testing marked environmental effects have been observed in the crack growth rate. The reason for this discrepancy is that at low corrosion potentials typical for PWR conditions, SCC cracks do not initiate or grow, but inside the CF cracks the crevice chemistry conditions prevail and the local environment at the crack tip can be very different from the bulk environment. It has been shown that local dissolution of MnS inclusions of the steel injects sulfur species into the crack-tip environment, including sulfides which even at ppm levels produce marked enhancement of the crack growth rate. This should be taken into account when SSRT tests are used for predicting the crack growth rates in reactor conditions.

In this SSRT testing program of A 516 Gr. 70 piping steel, the above mentioned discrepancies are avoided as much as possible in order to more accurately simulate the corrosion fatigue crack-tip conditions. Instead of using as-received material, prefatigued materials were used, which represent the material structure anticipated in the crack-tip process zone and in the area of maximum tensile stress ahead of the crack tip. The SSRT tests are performed both in the inert and bulk PWR environments as well as in the simulated crack-tip

environment corresponding to equilibrium dissolution of MnS in PWR-conditions. Both smooth and notched specimens are used so as to produce the multiaxial stress state which exists at the crack tip. The maximum possible crack growth rates are expected to be obtained for the material having the strain history of the corrosion fatigue crack tip subjected to the chemical and electrochemical conditions simulating the real crack tip as well as possible.

Also, the common use of as-received, unstrained materials in laboratory test programs does not take into account that the materials under plant operation are subjected to long and complex load histories. Therefore the laboratory data may not efficiently represent the in-service material properties. This study also addresses this issue.

3. EXPERIMENTAL METHODS

3.1 Test Material

The piping steel studied was A 516 Gr. 70 steel pipe [940 mm x 83 mm (37 in. x 3.25 in.] with chemical composition shown in Table 1. The mechanical properties of the piping steel are presented in Table 2. A generalized cutting diagram of A 516 Gr. 70 piping steel specimens is presented in Fig. 1.

Table 1 Chemical Composition (wt. %) of the A 516 Gr. 70 Steel Pipe

C	Mn	P	S	Si	Ni	Cr	Mo	Cu	V	Al
0.260	1.060	0.009	0.012	0.220	0.093	0.600	0.022	0.130	0.003	0.028

Table 2 Mechanical Properties of the A 516 Gr. 70 Piping Steel at Different Temperatures

Specimen ID	Orientation	Temp (°C)	Yield Stress (MPa)	UTS (MPa)	Area Red. (%)	Elongation (%)
F34-1	Longitudinal	22	257.0	499.0	18	24
F34-2	Longitudinal	22	270.0	514.0	18	24
F34-3	Longitudinal	149	241.0	451.0	67	29
F34-4	Longitudinal	149	237.0	446.0	67	29
BL-I2	Longitudinal	288	230.2	484.4	64	33
BL-M2	Longitudinal	288	210.4	509.5	60	31
BL-02	Longitudinal	288	263.8	494.4	64	30

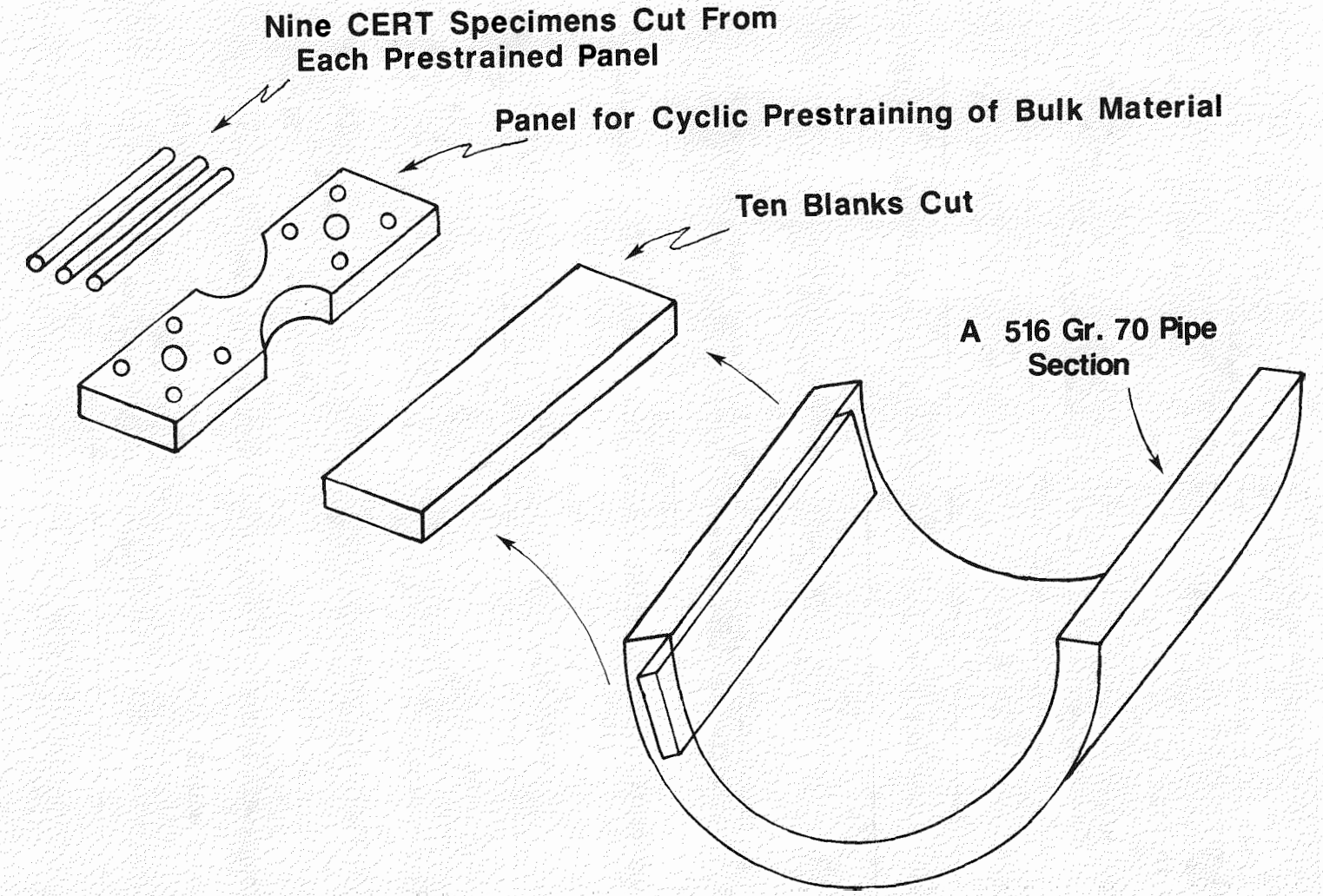

Fig. 1 Cutting diagram for prefatigue and SSRT specimens from A 516 Gr. 70 pipe section.

3.2 Cyclic Prestraining

Cyclic prestraining was performed by using large panel specimens on two MTS test systems rated to 550 kN (110 kip) and 2500 kN (500 kip) (Fig. 2). The cyclic straining tests were conducted at 288°C (550°F) in a stroke-controlled mode in case of high cyclic strain range and in a strain-controlled mode in case of low cyclic strain range. Axial strain was measured in the case of low cyclic strain range by a high temperature clip gage attached to the specimen. The load vs. strain/stroke data were plotted by an XY plotter.

Specimens were prefatigued in fully reversed axial strain cycles using a sinusoidal wave form. The maximum strain (i.e., the cyclic strain amplitude) was either 20% or 2%, and the corresponding mean strain values were 10% or 1%. As a cyclic frequency, 0.017 Hz (one cycle per minute) was used. The applied average strain rates for the prefatigue tests were equal to 6.7×10^{-3} s^{-1} and 6.7×10^{-4} s^{-1} respectively. No buckling took place in the specimens even in high cyclic strain range fatigue. However, in this case slight necking in the gage length was observed after fatigue. The number of applied cycles for the materials fatigued in the high cyclic strain was 25, and in the low strain range it was 100. Both materials were essentially cyclically stable after five initial cycles, and after that the maximum load increased only slightly. It can be considered that in case of high strain range, 25 cycles represent about the middle of the fatigue life, since one piping steel panel specimen cracked after 34 cycles, but in this case, the fatigue crack initiated from a thermocouple spot weld, which was erroneously placed on the gage length; a second trial piping steel specimen cracked after 50 cycles. Prefatigue was stopped at zero strain, i.e., in maximum compression, and the specimens were then unloaded. In case of high strain range, where stroke was used as controlling the fatigue process, the actual strains may be smaller than intended values, since some slipping of the specimen in the grips was taking place under high stresses. The magnitude of slipping could not be traced back, and its effects on strain and strain range values are not exactly known.

3.3 SSRT-Specimen Preparation

Following cyclic prestraining, the panel specimen was machined into SSRT specimens (Fig. 3). From each prefatigued panel specimen six SSRT specimens were obtained. The reduced gage section and the notch in the SSRT specimens are centered in the fully plasticized gage length of a prefatigued panel specimen. The type of notch used was that shown in Figure 3, with a 60° angle and a 0.007-in. notch root radius, giving a K_t factor of about 2 according to Peterson, (Ref. 36).

3.4 SSRT-Testing Conditions

SSRT testing was conducted in small autoclaves made of zirconium (Fig. 4). The specimens were electrically isolated from the autoclave body by using oxidized (550°C for 6 h) Zr retaining rings for the seals. This made the external potential control possible during

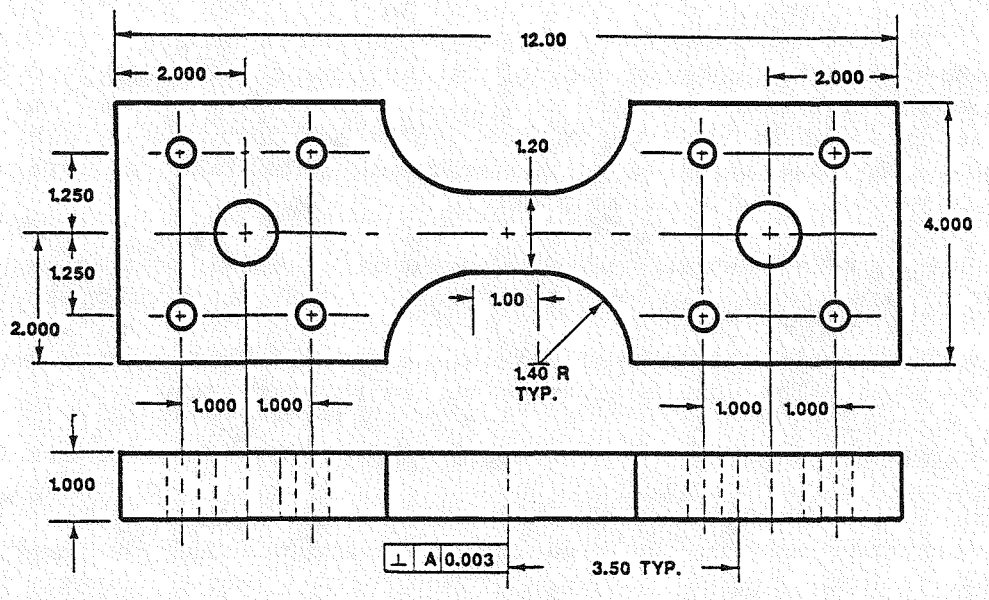

1 in. = 25.4 mm

GRINDING DIRECTION

Fig. 2 Specimen used to cyclically prestrain the piping steel. This large specimen was subsequently converted into SSRT specimens.

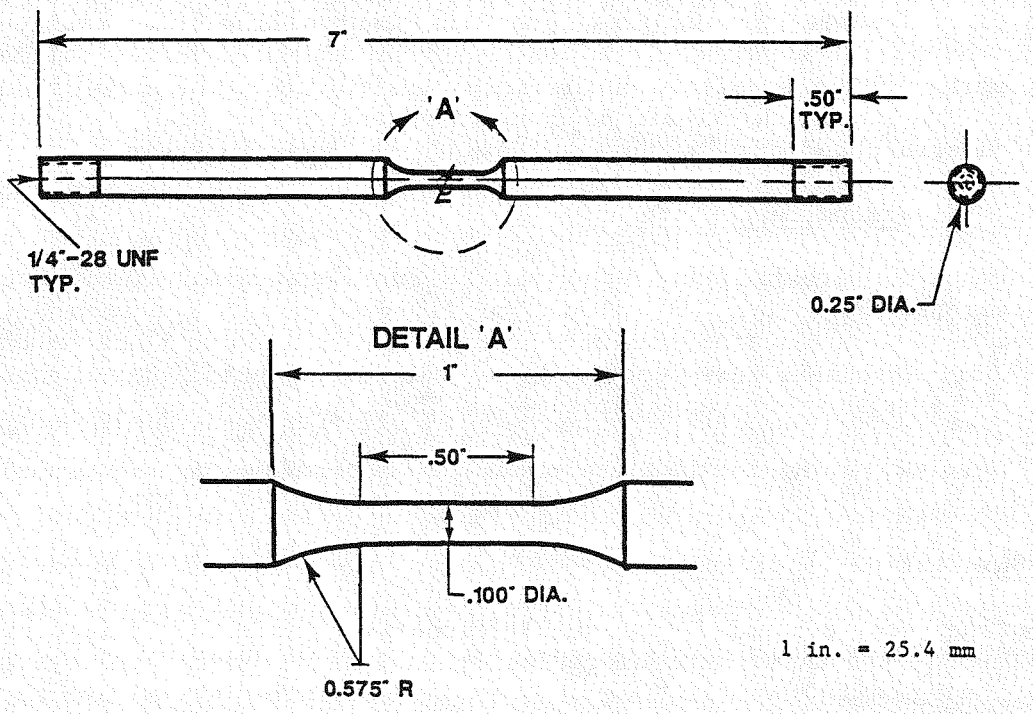

1 in. = 25.4 mm

Fig. 3 Slow strain rate test specimen used in this study.

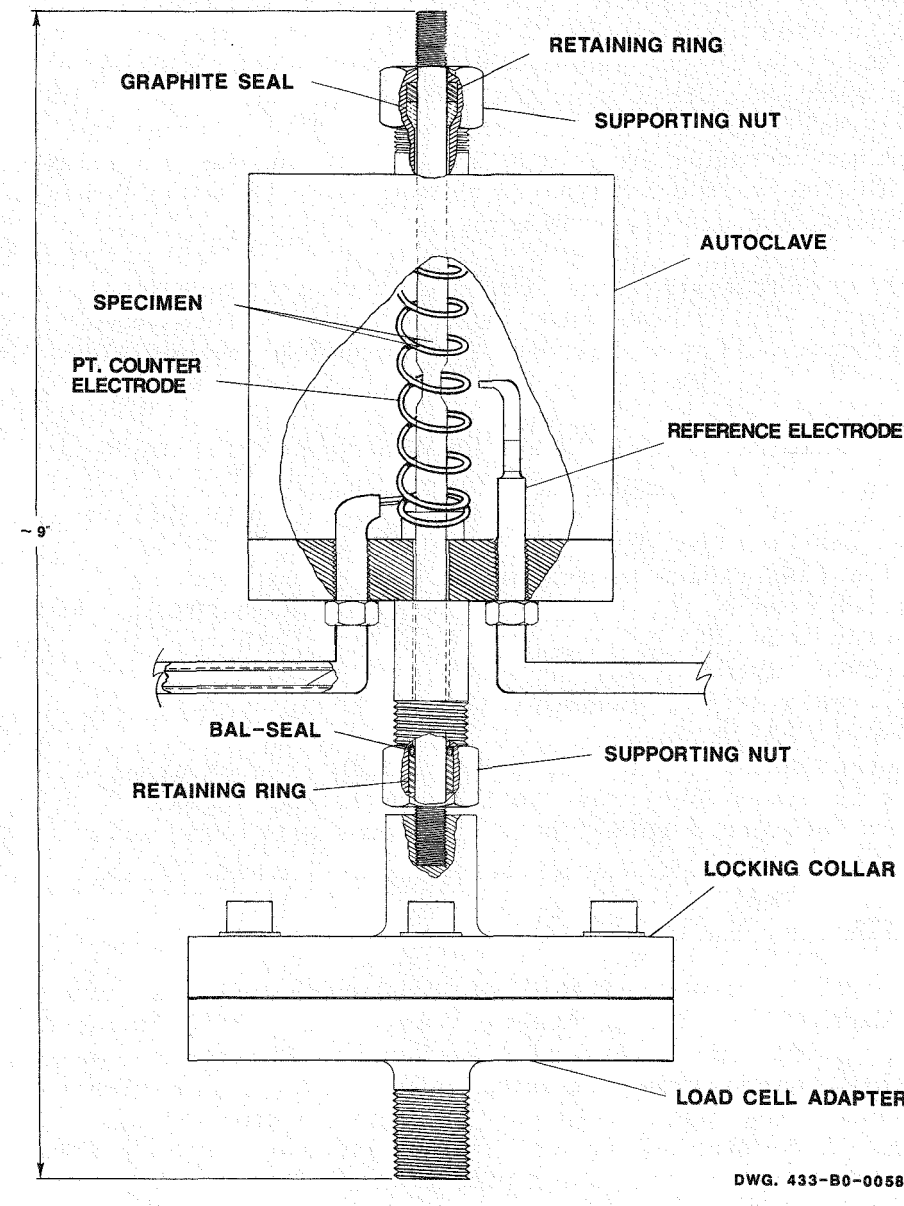

Fig. 4 Schematic of the autoclave used in the SSRT program.

SSRT testing. In all the measurements, the corrosion potential was measured by external Ag/AgCl reference electrodes. As a counter electrode, a wire-form electrode made of Pt-Rh alloy (Engelhard, Carteret, NJ) was used (Fig. 4). For controlled-potential testing, EG&G Princeton Applied Research potentiostat Model 362 was used. The experiments were performed in deoxygenated PWR primary water (Table 3) and in MnS contaminated PWR primary water, which contained the equilibrium solubility of MnS at the test temperature and conditions. MnS was packed into a crevice formed by heat-shrink Teflon up to about 3/4 of the gage length so that the notch in the middle of the gage length was covered by MnS. This ensured electrical contact between the steel and the MnS as is the case inside the CF crack when MnS inclusions are uncovered. A deoxygenated aqueous environment was obtained by evacuating the piping and autoclave, which were then filled with deoxygenated water from the water make-up tank, which was under nitrogen gas pressure.

Most of the SSRT tests were carried out at the strain rate of 3.5×10^{-7} s^{-1}, but in some tests also 7×10^{-7} s^{-1} was used. Straining was started when a low stable corrosion potential value was obtained.

Table 3 Nominal Water Chemistry Specification

Boron (as boric acid)	1000 ppm
Lithium (as lithium hydroxide)	1 ppm
Chloride ions	< 0.15 ppm
Fluoride ions	< 0.10 ppm
Dissolved oxygen	~ 1 ppb
Dissolved hydrogen (saturation)	30 to 50 cm^3/kg water

All other metallic or ionic species should be at about trace levels. Some iron, both in solid and soluble form is the inevitable result of a corroding specimen.

3.5 Analysis of the Test Results

SSRT-test results were analyzed in the same way as tensile test results. Elongation to fracture (A) was obtained from nominal strain rate and the test time. Before starting the SSRT tests, the nominal strain rate obtained from the motor speed and gear ratios was calibrated with an LVDT and a clip gage which were in good agreement with each other. Reduction of area (Z) was measured directly from smooth specimens by using a traveling microscope; in the case of notched specimens, SEM pictures of the fracture surfaces were used to compute Z. The equivalent plastic strain at fracture initiation, $\bar{\epsilon}_f^p$, was also calculated ($\ln (S_o/S)$) where S_o and S are the initial and final projected surface area. In case of notched specimens, no attempts were made to calculate the notch opening, the change in the notch root radius of curvature or the change in the notch angle, parameters which could have been also used in estimation of the equivalent plastic strain at fracture. The yield stress, σ_y, and the ultimate tensile

strength, σ_m, values were obtained directly from the load-time curves plotted by an XY plotter. Because of the relatively low resolution of this large strain plot, the yield stress was determined from the load where the curve deviated from the Hookean law straight line. For notched specimens, the stresses are net section stresses calculated for the area at the bottom of the notch. This was thought to be a reasonable approximation for the stress, since the stress concentration factor can only be used to calculate the maximum stress in the notch root, and it does not provide any information about the stress distribution in the cross-section of the notch root region.

The microstructure of the prefatigued specimens was determined by using transmission electron microscopy (TEM). After SSRT testing, the specimens were studied fractographically to reveal the fracture mode. In cases of SCC crack growth, the maximum crack length was measured and the crack growth rate was determined by anticipating that the crack growth started from the notch root at the yield stress. This procedure is believed to result in a reasonable estimate of maximum crack growth rate in different materials in the simulated crack-tip environments and under controlled electrochemical potentials (ECP). After SSRT-testing (about 6 months later) the residual hydrogen contents were measured in some specimens by cutting a sample containing the fracture surface and most of the gage length. For measurement a Leybold-Hereaus Model H2A 2002 test system based on thermal conductivity was used.

4. RESULTS

4.1 Cyclic Prestraining

The cyclic stress-strain curves of A 516 Gr. 70 piping steel are presented in Figures 5a and 5b. When the number of cycles increases, the cyclic stress-strain curve is higher, as compared to previous curves or first cycle, indicating characteristics of cyclic hardening. Cyclic hardening is more evident in the case of the small 2% strain amplitude, Figure 5a. In the case of high strain amplitude (nominally 20%), the lower values of stress when strain is small are most probably due to slipping of the large specimens in the grips. When the strain is high, slight cyclic hardening can be observed. Possible slipping in the grips reduced the maximum strain achieved during fatigue of high cyclic strain panel specimens where stroke-control was used for applying and measuring the strain. However, the amount of this was very difficult to estimate.

4.2 Microstructures

The metallographic structures of as-processed (unstrained) and cyclically prestrained A 516 Gr. 70 specimens are shown in Figure 6. Following cyclic prestrains no details of the microstructure in optical micrographs do appear more distinguished, as compared to as-processed unstrained material. The typical ferritic-pearlitic microstructure can be observed with ferrite grain size of ASTM No. 8 corresponding to an average grain size of 22 μm.

Transmission electron microscopy (TEM) studies indicated that unstrained A 516 Gr. 70 steel had a low dislocation density in the ferrite, Figure 7a to 7c, and the dislocations were straight and showed some knitting into dislocation networks. Inside pearlite the cementite lamellae seemed to pin dislocation lines which formed straight lines between the cementite lamellae, Figure 7d. This structure is typical for carbon steels after slow-cooling heat treatment.

Maximum cyclic strain of 2% produced an equiaxed (average cell size 0.7 μm to 1 μm) dislocation cell structure through the ferrite phase, Figures 7e and 7g. Almost all dislocations were tangled into the cell walls and inside the dislocation cells only very few dislocations were present. During cyclic loading individual dislocations are only able to propagate distances of the order of the cell wall spacing, in this case of the order of 1 μm. Inside pearlite the dislocation density had only slightly increased, Figures 7f and 7h. Cementite lamellae have pinned more dislocations, which can be seen especially at the phase boundaries in Figure 7h.

High maximum cyclic strain, nominally 20%, had resulted in highly dislocated microstructure, Figures 7i and 7j. In this case both ferrite and pearlite had deformed. In the ferrite, the cell size (where it is discernable) had decreased to 0.5 μm to 0.7 μm. However, there were areas in the microstructure which contained high amounts of evenly distributed dislocations through the matrix. Also the cell

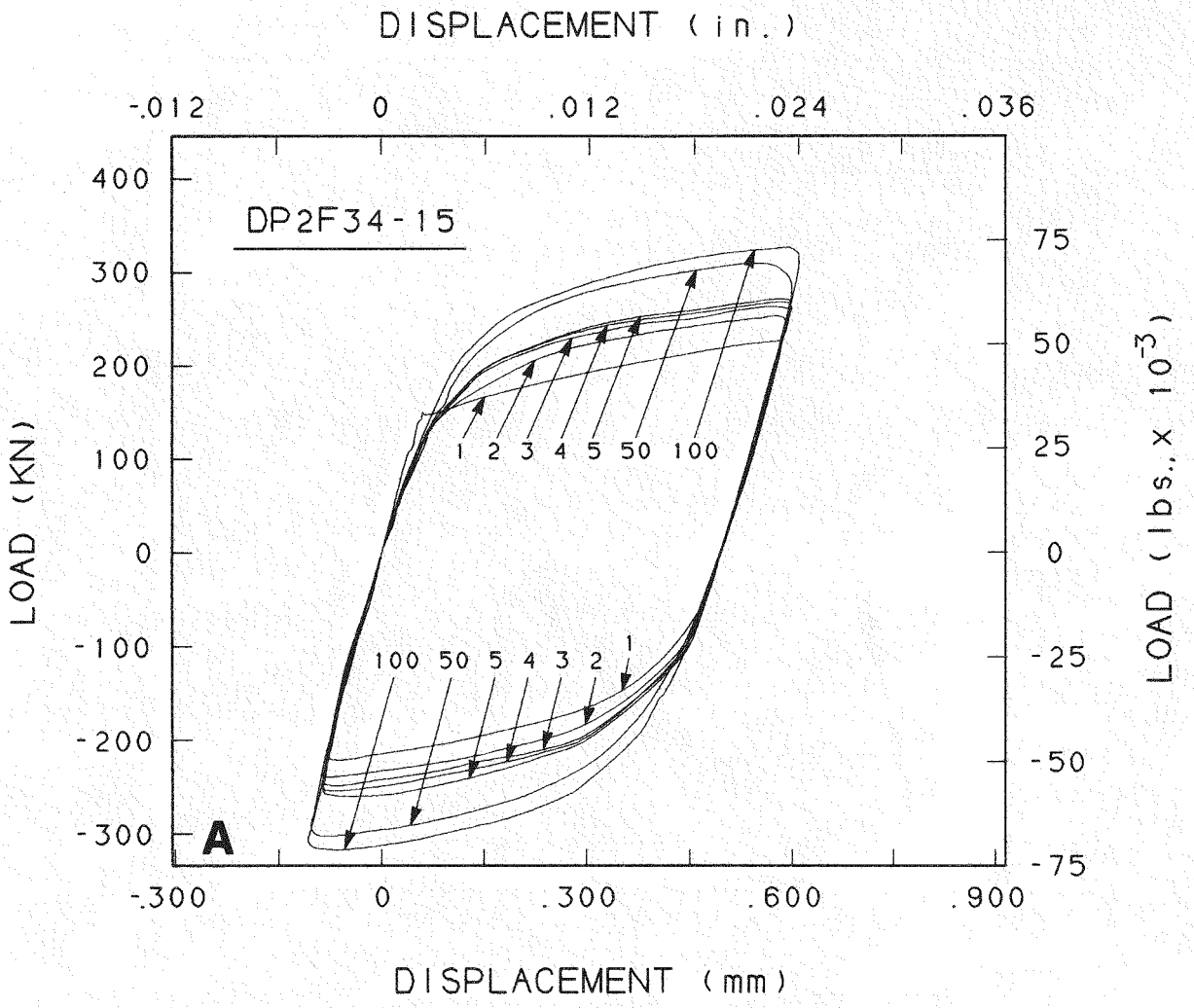

Fig. 5 Cyclic stress-strain curves of A 516 Gr. 70 piping steel large panel specimens: (a) maximum strain 2%, and (b) maximum nominal strain 20%. The numbers indicate the cyclic count. The shape of the hysteresis curves of highly strained material (b) are possibly affected by shipping in the grips in the area of the smaller strains.

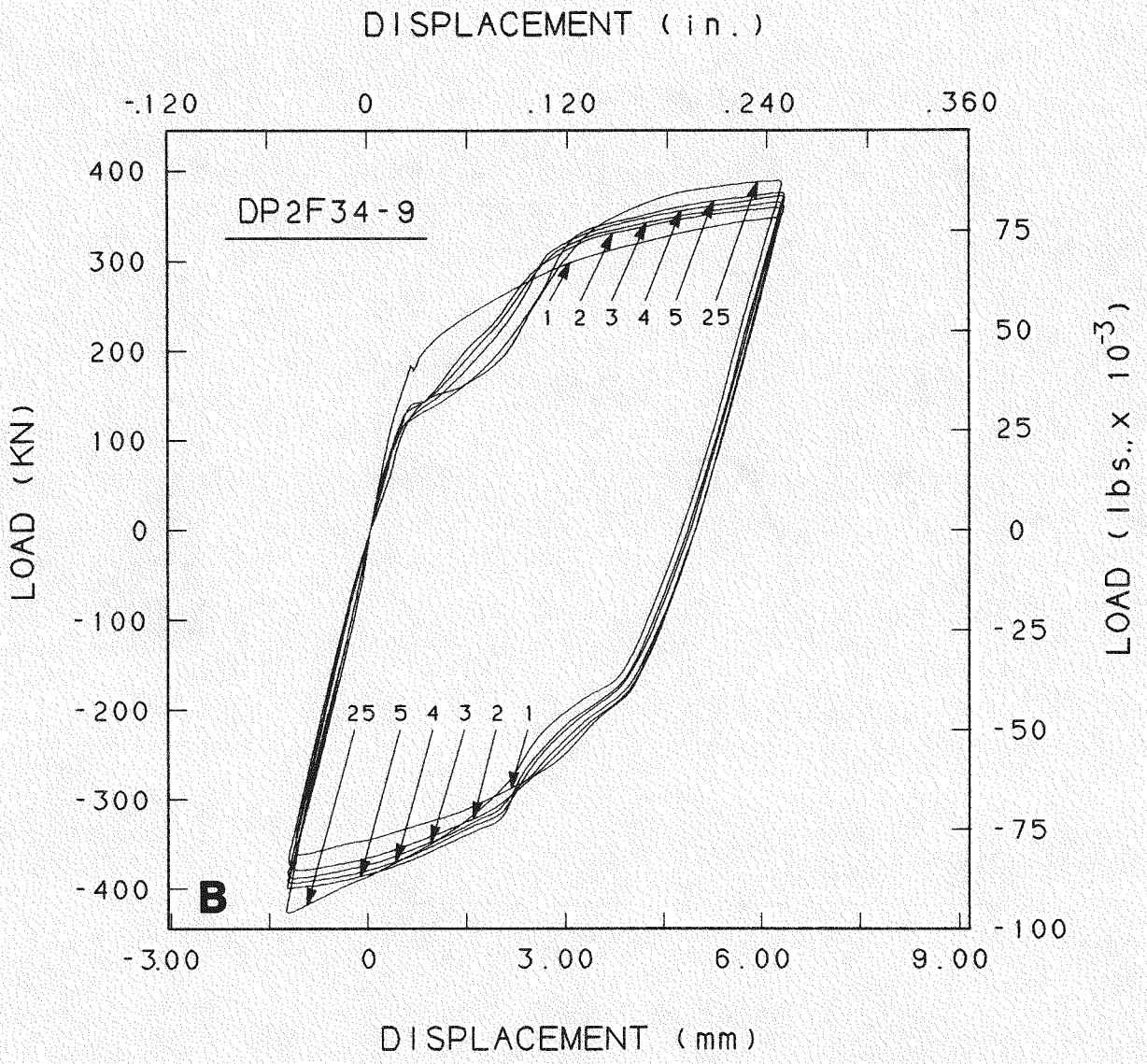

Fig. 5. (continued)

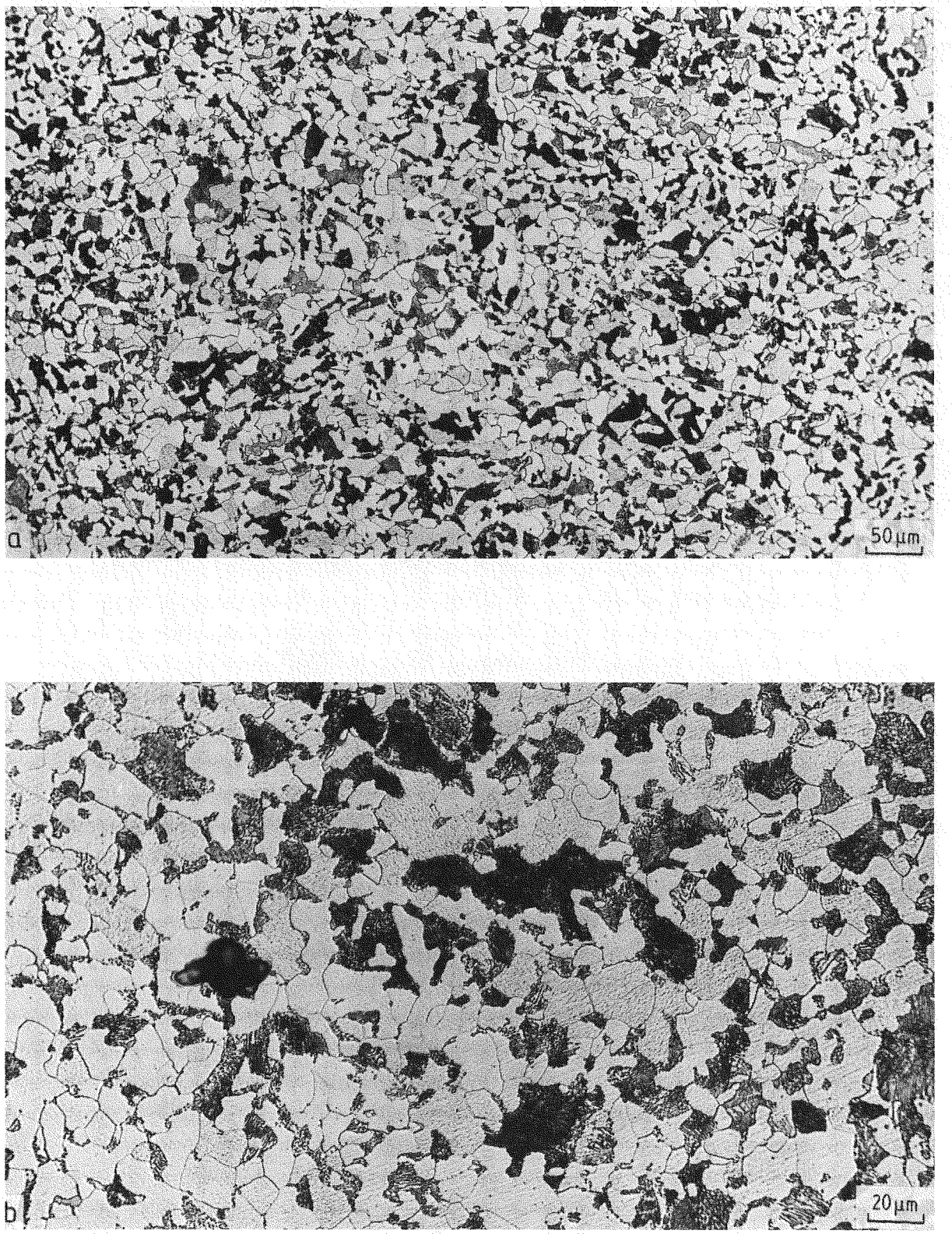

Fig. 6 Optical microstructures of as-processed unstrained and cyclically prestrained A 516 Gr. 70 steel: (a) and (b) unstrained, (c) and (d) 2% maximum strain (100 cycles), and (e) and (f) 20% nominal maximum strain (25 cycles).

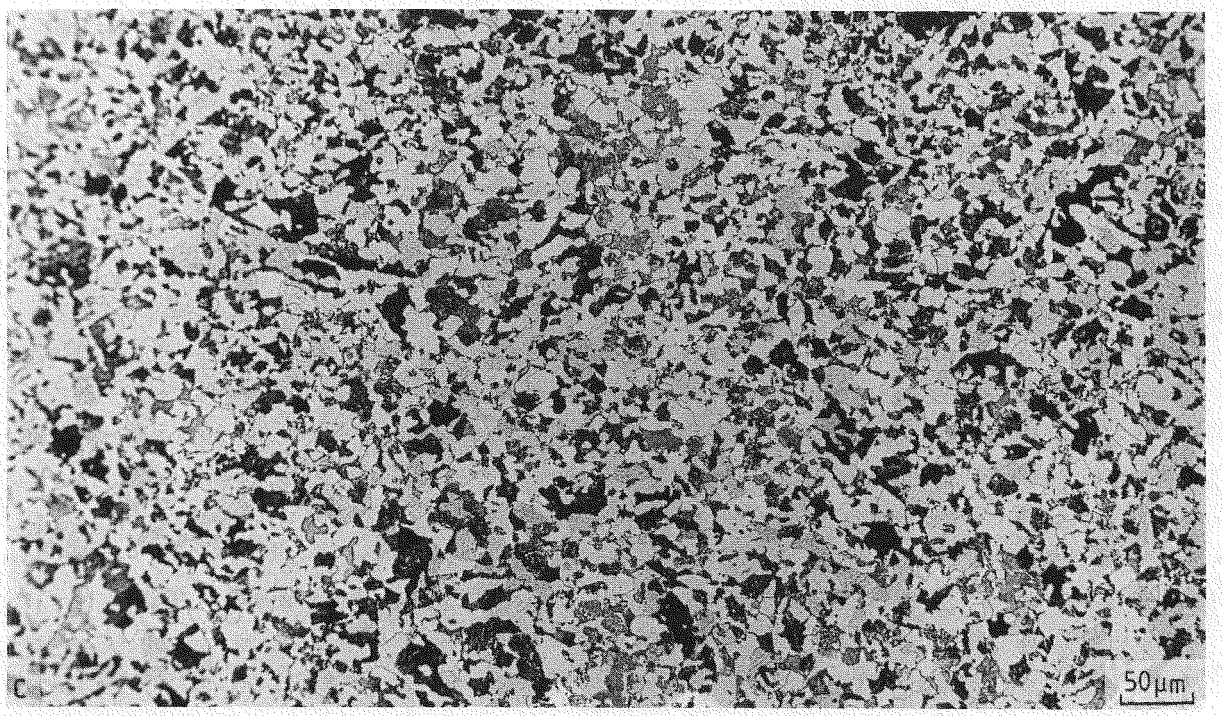

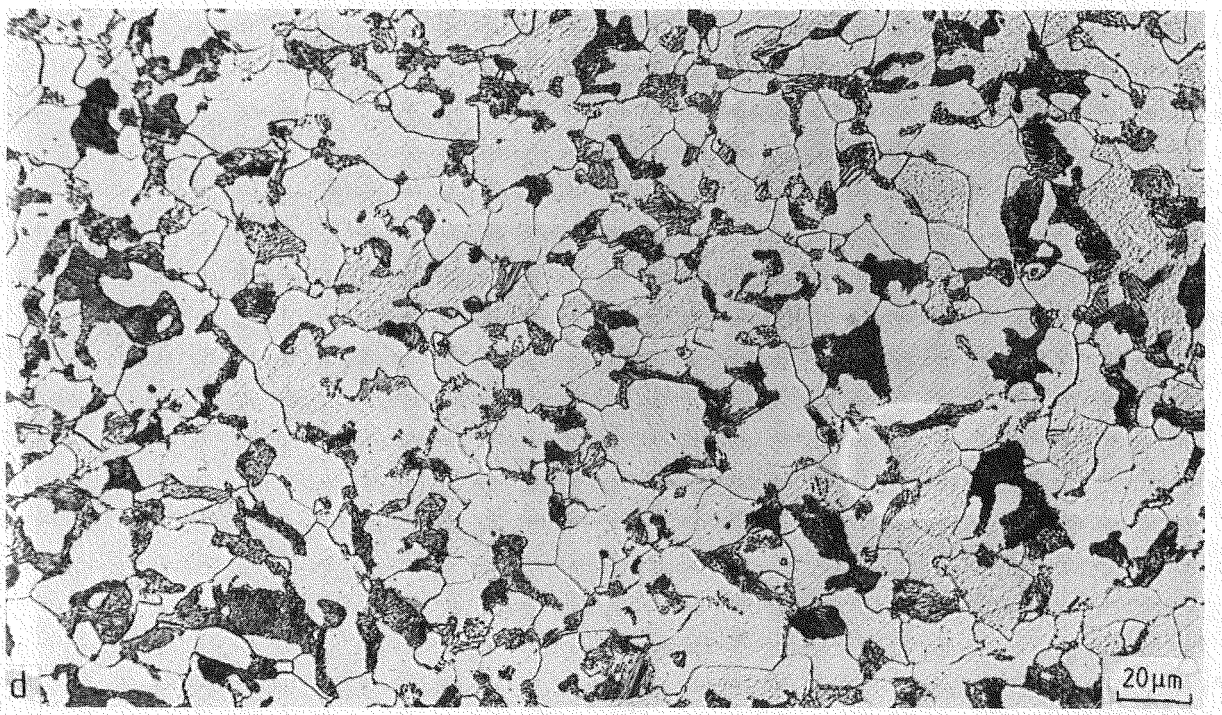

Fig. 6. (continued)

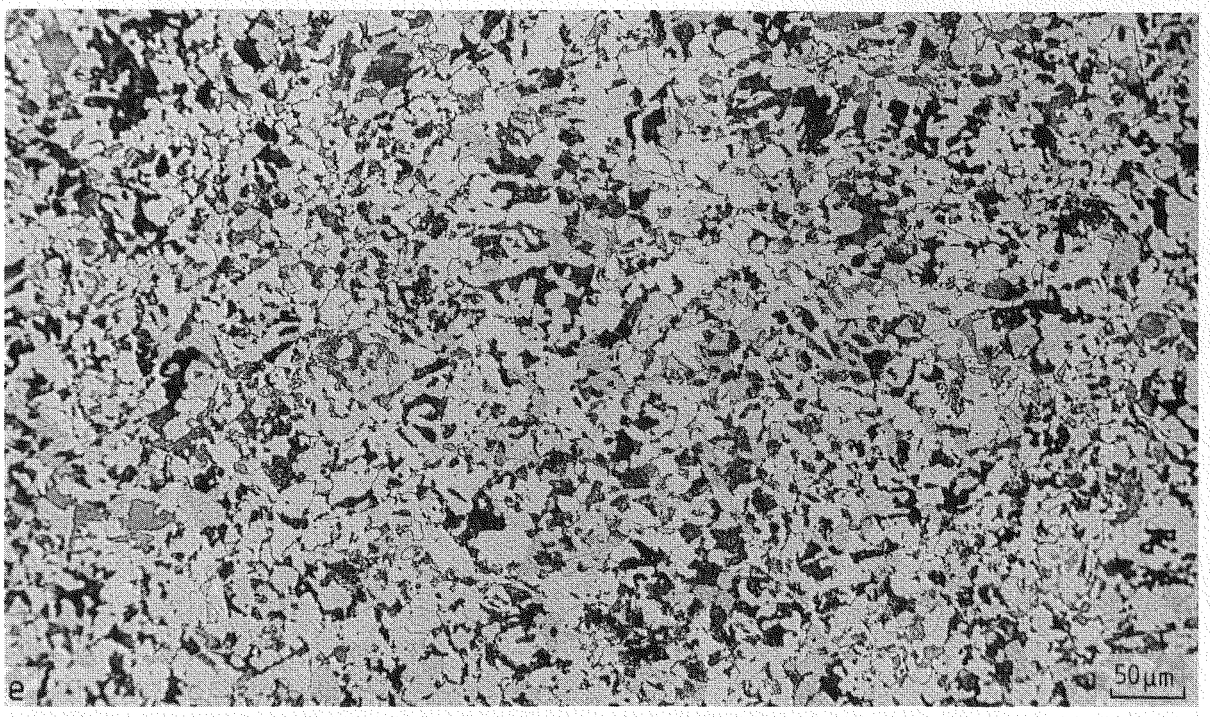

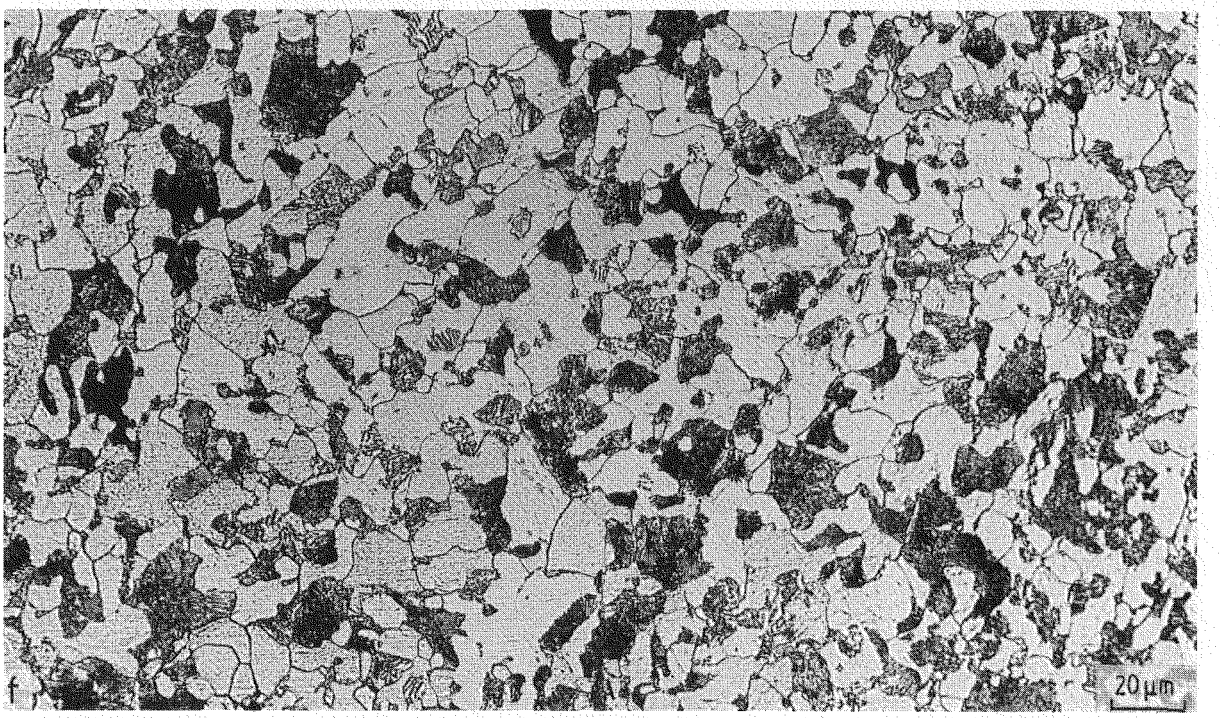

Fig. 6. (continued)

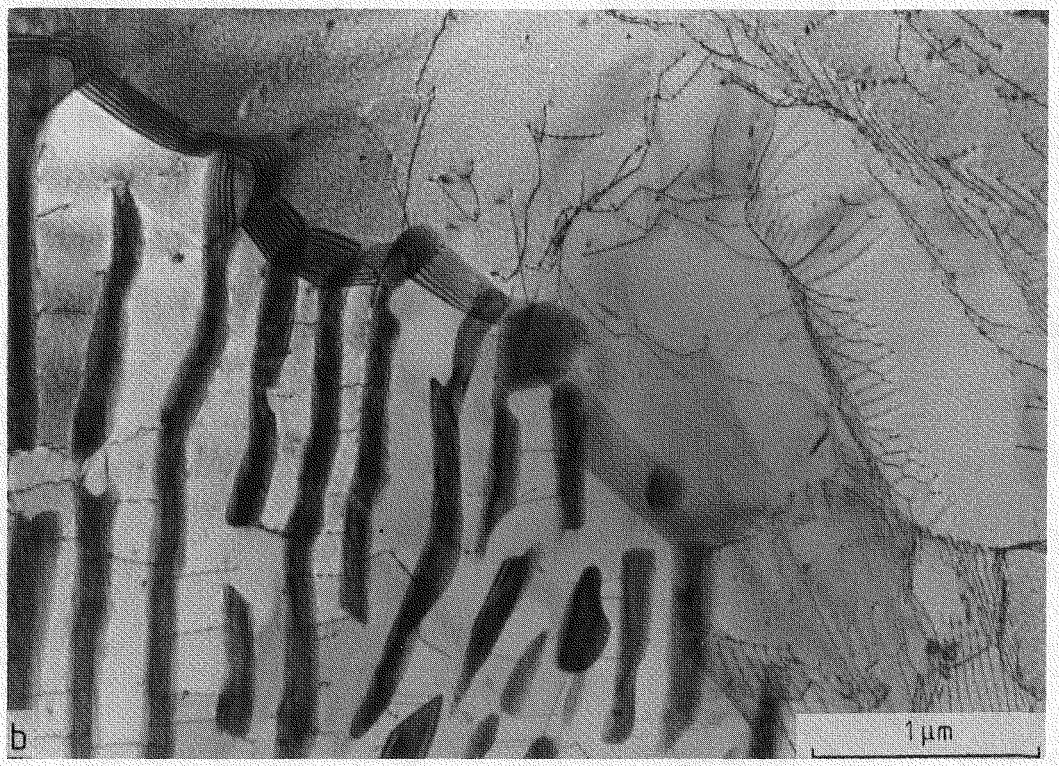

Fig. 7 Transmission electron microscopy microstructures of as-processed and cyclically prestrained A 516 Gr. 70 steel: (a) through (d) as received, unstrained; (e) through (h) 2% maximum strain (100 cycles); and (i) through (l) 20% maximum strain (25 cycles).

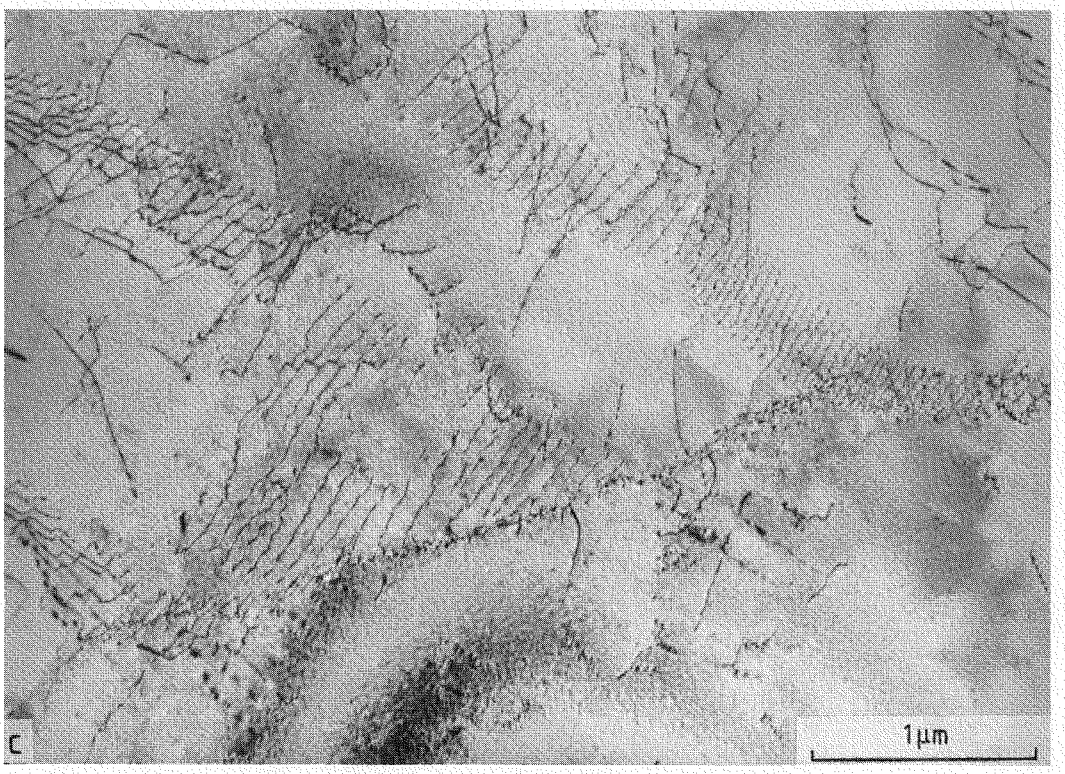

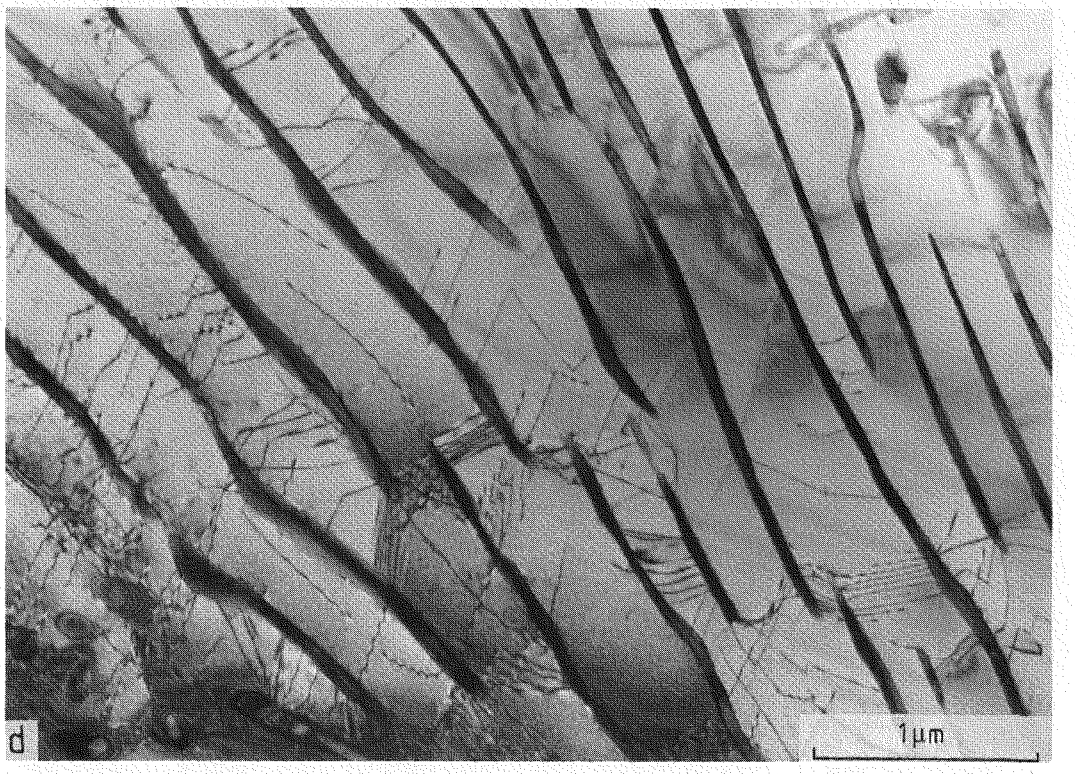

Fig. 7. (continued)

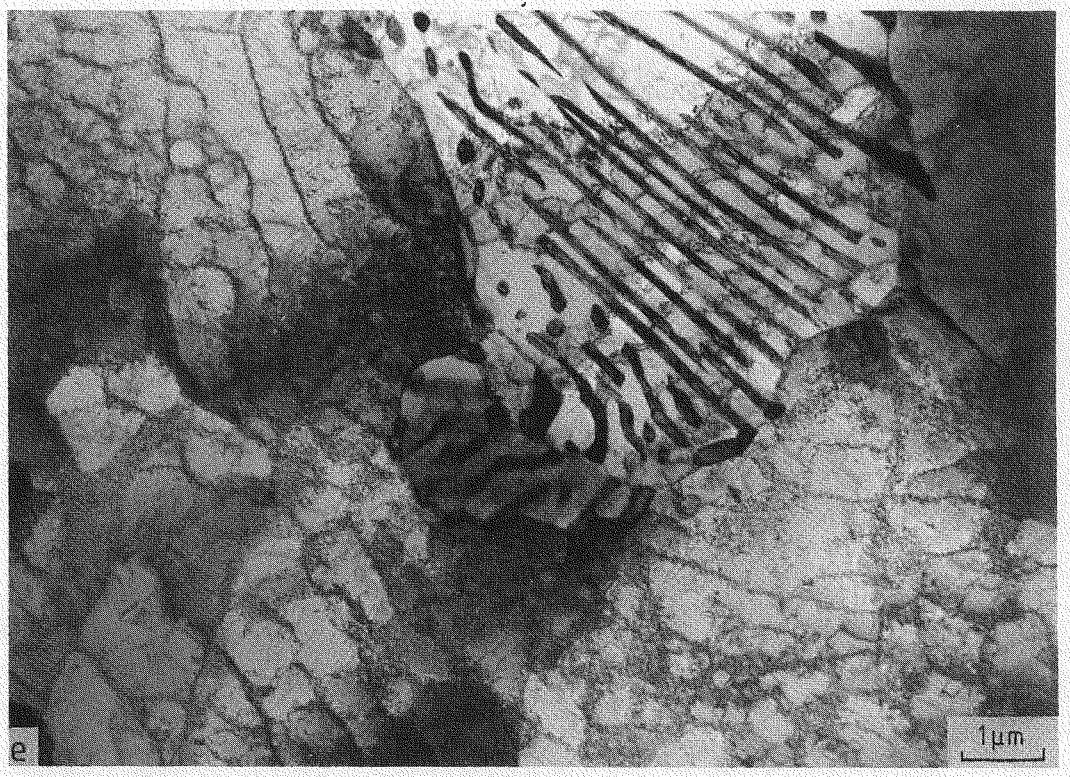

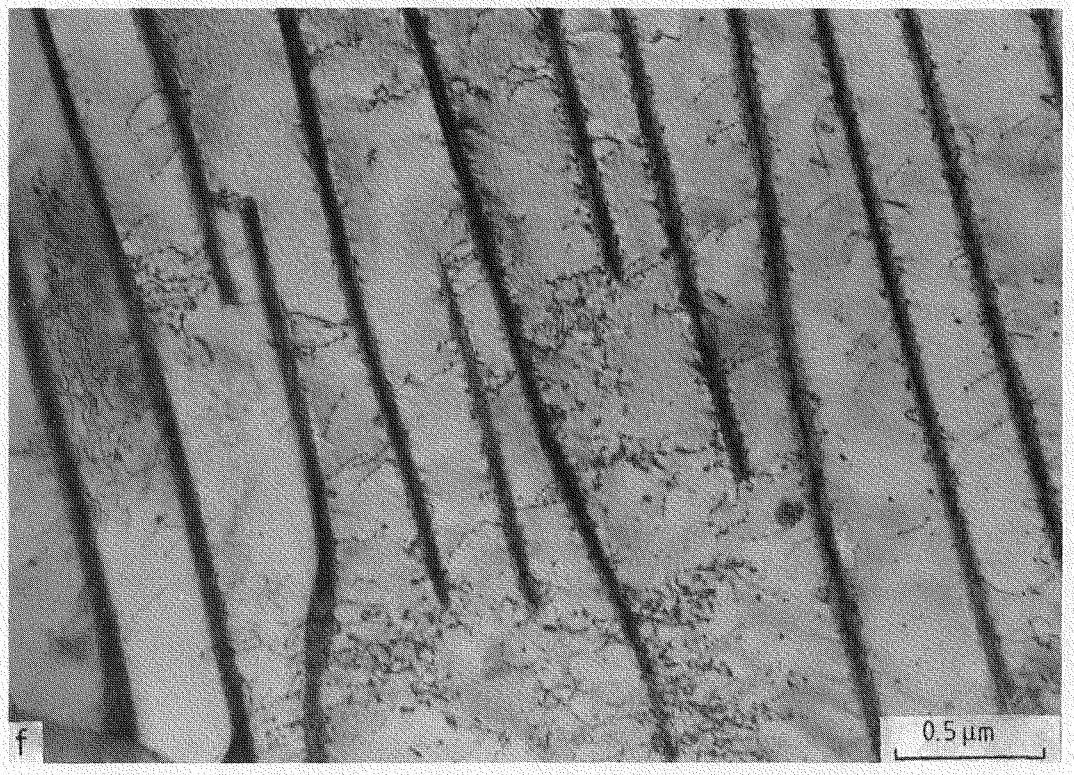

Fig. 7. (continued)

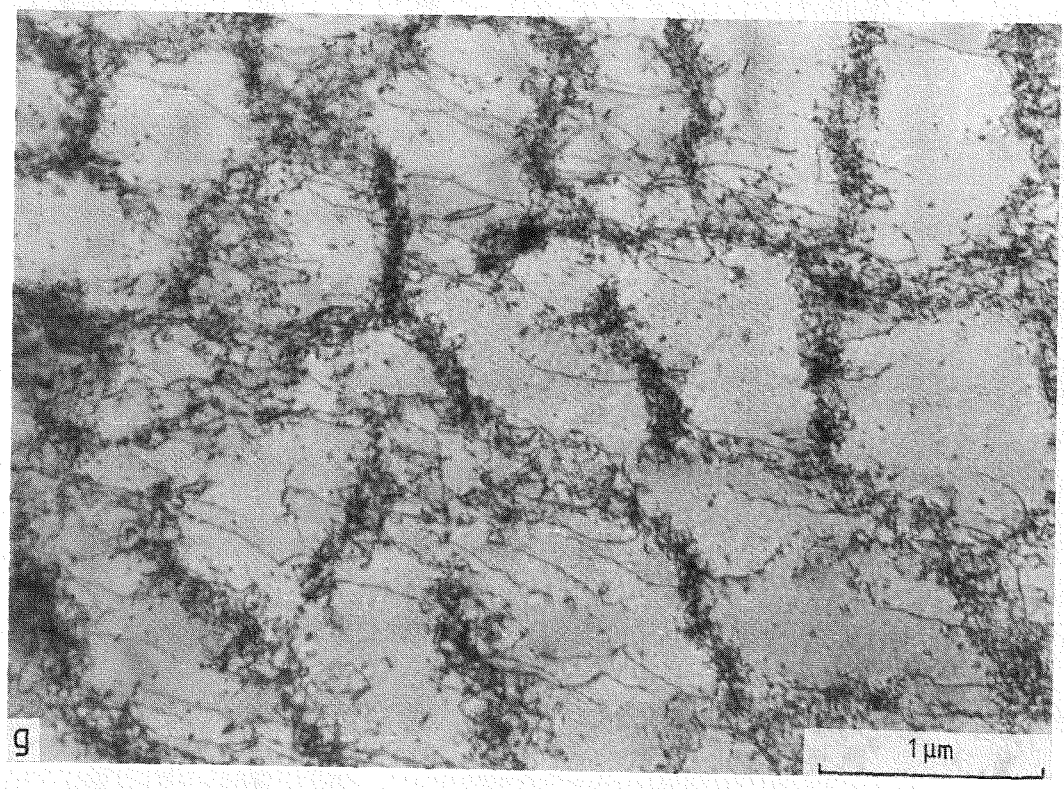

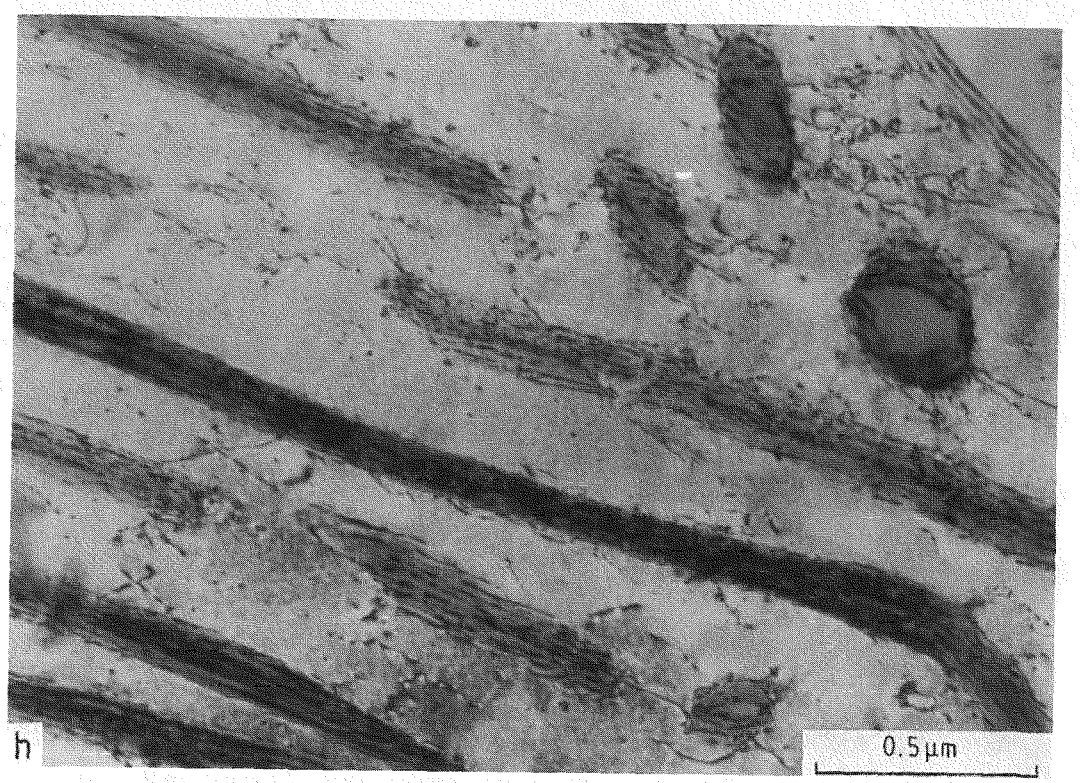

Fig. 7. (continued)

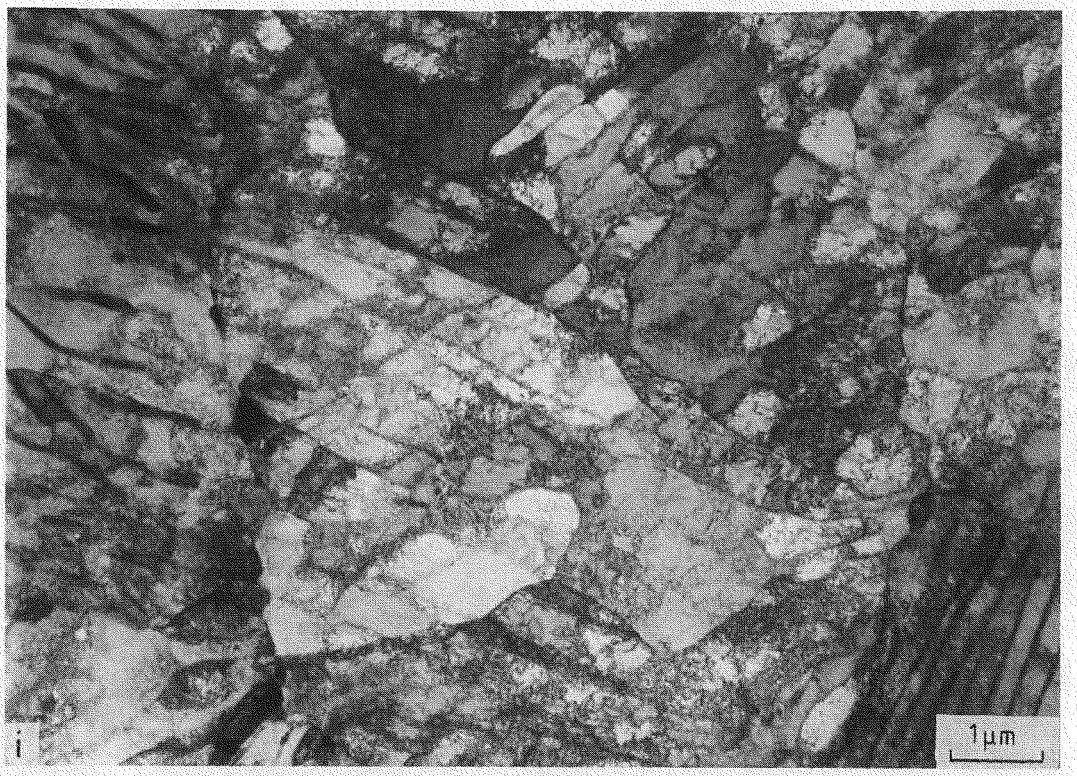

Fig. 7. (continued)

Fig. 7. (continued)

walls in this material were much thicker, as compared to 2% maximum strain material. This material also contains cells which were not usually equiaxed, but exhibited the structure of an elongated cube, Figures 7j and 7k. Inside regions of pearlite the spacings between cementite lamellae were now full of tangled dislocations, the density of which showed some local differences. No clear dislocation cell structure could be discerned in the pearlite, Fig. 7l.

4.3 Slow Strain Rate Tests

The SSRT-test results in helium, pure water, bulk and MnS-contaminated PWR water for A 516 Gr. 70 piping steel in the as-received condition and in prefatigued conditions are presented in Table 4. It can be seen from this table that the notch with $K_t = 2$ markedly increased the yield stress and the ultimate tensile stress of the specimens and reduced the elongation to fracture. The best mechanical properties were obtained in helium, where prefatigued notched specimens with 10% mean strain showed the highest elongation to fracture of all the notched specimens. In pure and PWR-water the stress and the elongation values behaved similarly with respect to the level of prefatigue. It seems that prefatigue does not affect the material mechanical properties in the SSRT-tensile test in conditions where SCC is not taking place.

In as-received, unstrained condition, A 516 Gr. 70 piping steel failed in a ductile manner in both deoxygenated pure and in deoxygenated PWR-water, Figs. 8 and 9. In MnS-saturated PWR-water, SCC took place, Fig. 10.

Low-strain, prefatigued A 516 Gr. 70 piping steel failed in deoxygenated, pure PWR-conditions at free corrosion potential always in a ductile manner, Fig. 11a. Cathodic polarization to -1500 mV(SHE) produced also ductile fracture, Fig. 11b, with reduced elongation to fracture and reduction of area. Anodic polarization to 0.0 mV(SHE) caused SCC in pure deoxygenated PWR-water Figs. 11c and 11d. Four SSRT tests were performed for low strain prefatigued A 516 Gr. 70 piping steel in MnS-saturated deoxygenated PWR-water. The corrosion potential was varying in each test; SCC occurred in three specimens, Figs. 12a to 12c are examples, but did not occur in the specimen having the lowest corrosion potential (E = -680 mV(SHE)), Fig. 12d. Also the crack growth rate of specimen having corrosion potential, E = -660 mV(SHE), was markedly lower than in case of the two other specimens which showed clear SCC. The SCC fracture surface was typical of environment-sensitive cracking of low alloy steels, Figs. 13 and 14. Polarization to 0.0 mV(SHE) in MnS-saturated PWR-water resulted in the highest crack growth rate in this testing series. In this case the fracture surface was strongly attacked, Figs. 15a to 15c. Cathodic polarization to -1500 mV(SHE) caused ductile fracture with reduced elongation to fracture and reduction of area, Fig. 15d.

High strain prefatigued A 516 Gr. 70 piping steel was very ductile in helium as well as in deoxygenated PWR-water at 288°C, Fig. 16. This material condition showed SCC both in MnS-saturated, deoxygenated PWR-water at free corrosion potential, E = -570 mV(SHE), Fig. 17, and

Table 4 Summary of the SSRT Test Results of the As-received and Prefatigued A 516 Gr. 70 Piping Steel Specimens in Helium, Pure Deoxygenated, Deionized Water, and Pure and MnS-contaminated Deoxygenated PWR Water

Environment	As-received Pre-strained	Smooth or Notched	Type of Test Potential	Corrosion Potential (V)	Yield Stress (MPa)	Ultimate Stress (MPa)	Elongation to Fracture (%)	Z	ln(S/So)	Failure Mode D - Ductile B - Brittle
Pure Water	As. Recvd.	Smooth	Free	-----	211	412	28.4	62.8	0.99	D
Pure Water	As. Recvd.	Notched	Free	-----	405	519	10.8	35.7	0.44	D
Pure Water	As. Recvd.	Notched	Free	-----	260	592	17.0	33.5	0.40	D
PWR Water	As. Recvd.	Smooth	Free	-----	192	424	26.6	69.4	1.18	D
PWR Water	As. Recvd.	Notched	Free	-----	265	488	16.4	41.7	0.54	D
PWR Water+MnS	As. Recvd.	Notched	Free	-0.65	207	467	8.3	17.4	0.19	B
PWR Water	Low-Strain	Notched	Free	-0.83	353	498	17.0	53.5	0.76	D
PWR Water+MnS	Low-Strain	Notched	Free	-0.66	301	509	14.1	41.9	0.54	B
PWR Water+MnS	Low-Strain	Notched	Free	-0.51	280	384	3.3	12.5	0.13	B
PWR Water+MnS	Low-Strain	Notched	Free	-0.68	332	530	18.8	53.5	0.77	D
PWR Water+MnS	Low-Strain	Notched	Free	-0.58	280	415	3.8	16.0	0.13	B
PWR Water	Low-Strain	Notched	Applied	0.00	290	363	2.4	7.2	0.08	B
PWR Water	Low-Strain	Notched	Applied	-1.50	343	509	11.3	35.8	0.44	D
PWR Water+MnS	Low-Strain	Notched	Applied	0.00	301	410	3.8	8.8	0.09	B
PWR Water+MnS	Low-Strain	Notched	Applied	-1.50	327	509	11.3	29.0	0.34	D
PWR Water+MnS	Low-Strain	Notched	Applied	-1.50	322	485	9.1	26.7	0.31	D
Helium	High-Strain	Smooth	—	-----	405	579	23.7	75.3	1.40	D
Helium	High-Strain	Notched	—	-----	415	654	19.5	39.8	0.51	D
PWR Water	High-Strain	Smooth	Free	-0.85	317	459	21.7	73.3	1.32	D
PWR Water	High-Strain	Notched	Free	-0.80	348	530	12.3	39.3	0.50	D
PWR Water	High-Strain	Notched	Free	-----	369	561	22.0	75.8	1.42	D
PWR Water+MnS	High-Strain	Notched	Free	-0.57	358	540	11.6	33.5	0.41	B
PWR Water+MnS	High-Strain	Notched	Applied	0.00	---	514	3.3	9.9	0.10	B
Pure Water	High-Strain	Smooth	Free	-----	---	462	18.9	65.0	1.05	D
Pure Water	High-Strain	Notched	Free	-----	---	533	15.2	32.0	0.36	D

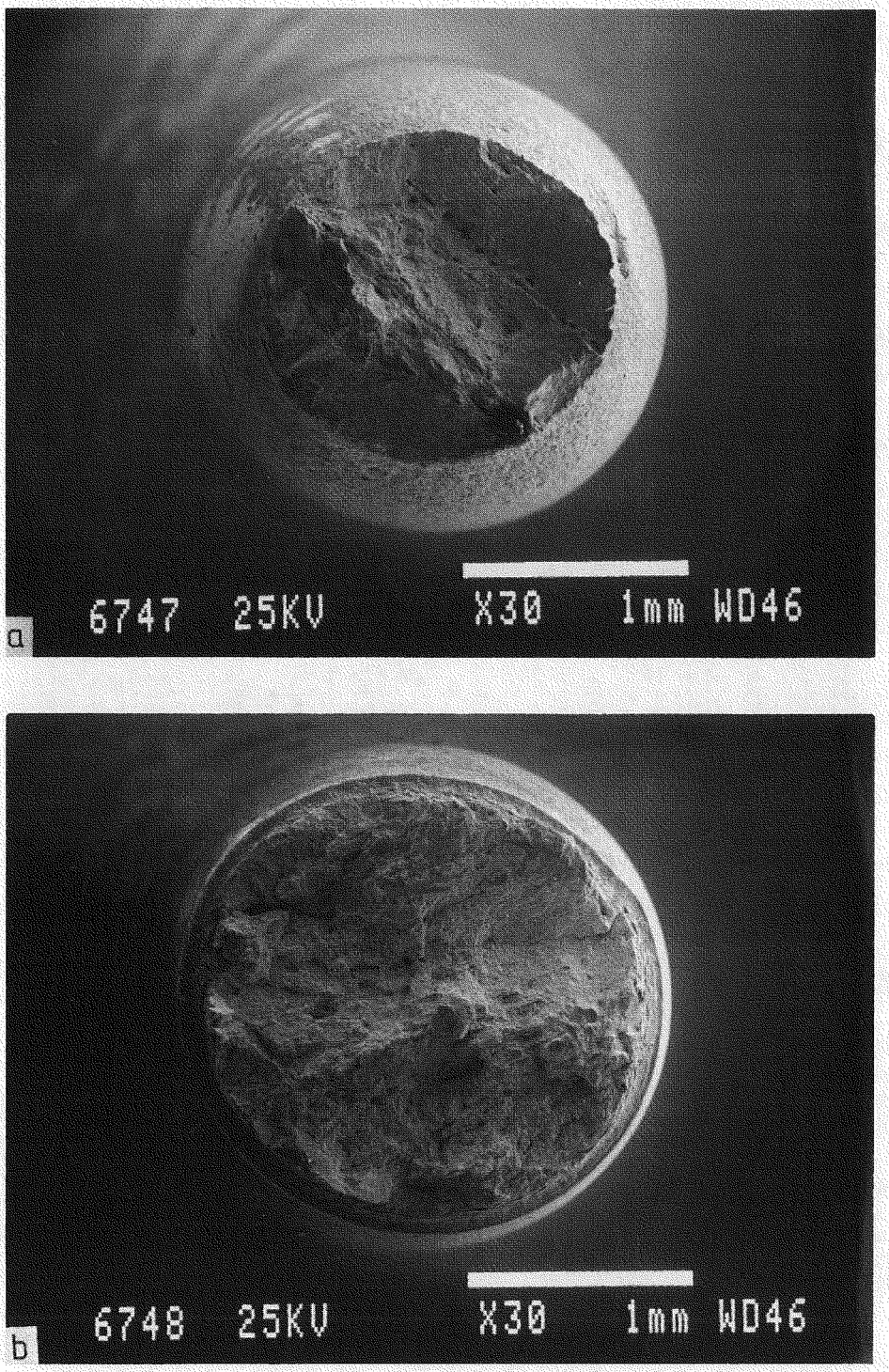

Fig. 8 Fracture surfaces of as-received unstrained A 516 Gr. 70 piping steel SSRT-specimens: (a) smooth specimen, and (b) notched specimen in deoxygenated pure water at 288°C.

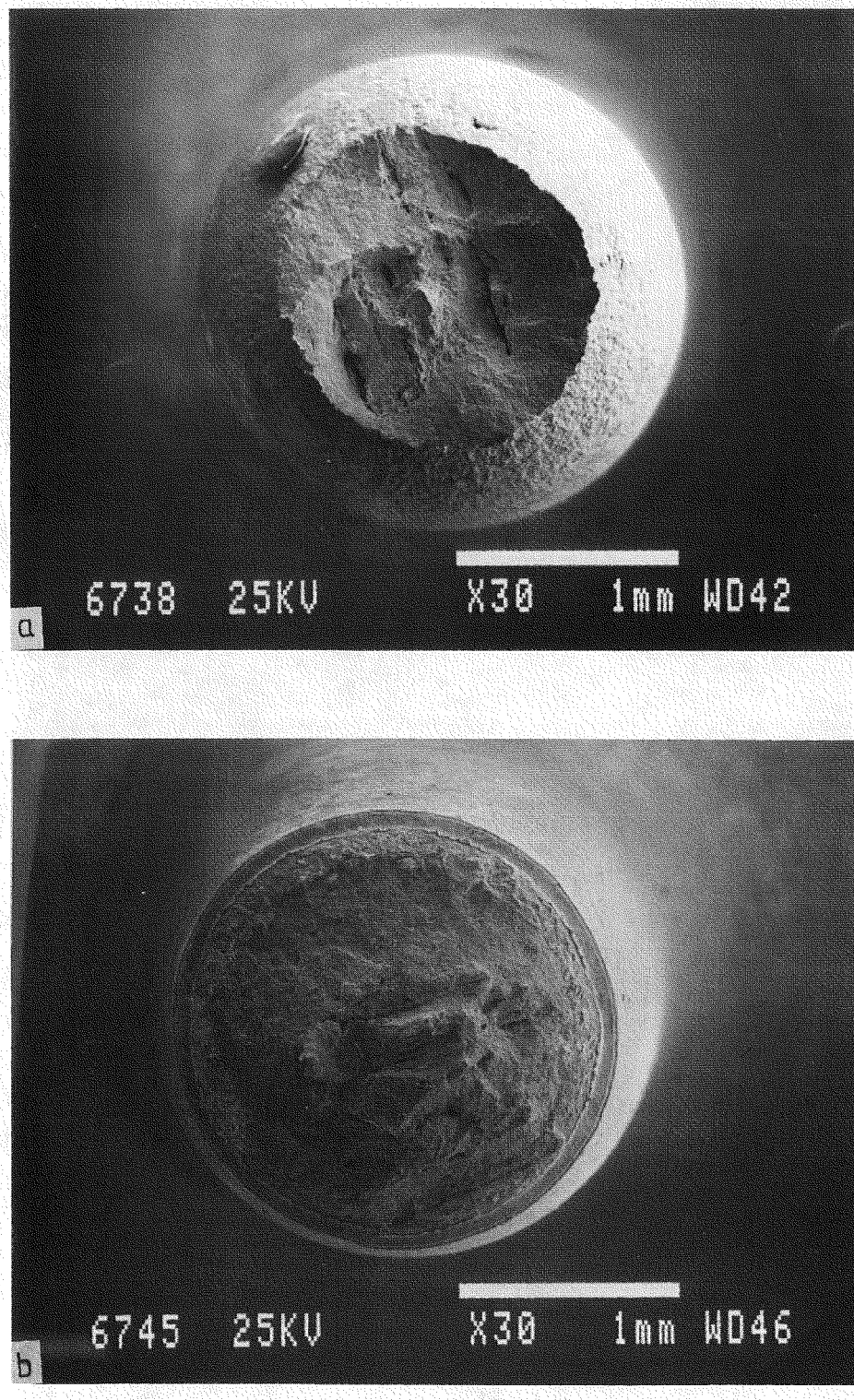

Fig. 9 Fracture surfaces of as-received unstrained A 516 Gr. 70 piping steel SSRT-specimens: (a) smooth, and (b) notched specimen in deoxygenated PWR-water at 288°C.

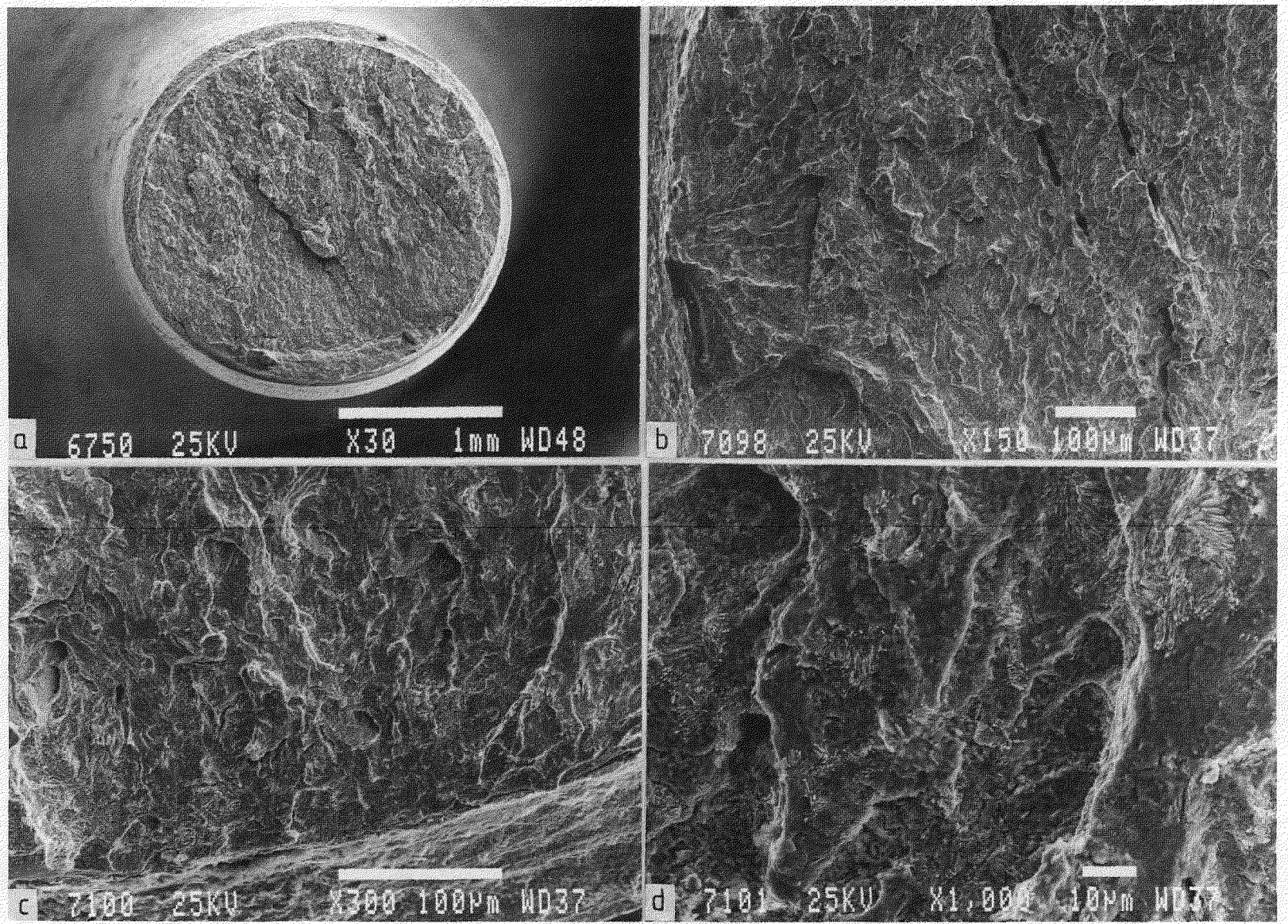

Fig. 10 Fracture surface of as-received unstrained notched specimen of A 516 Gr. 70 piping steel tested in MnS-saturated PWR Water (E = -650 mV(SHE)) at 288°C. Note almost complete penetration of specimen by SCC and that the fracture surface has been attacked by the environment.

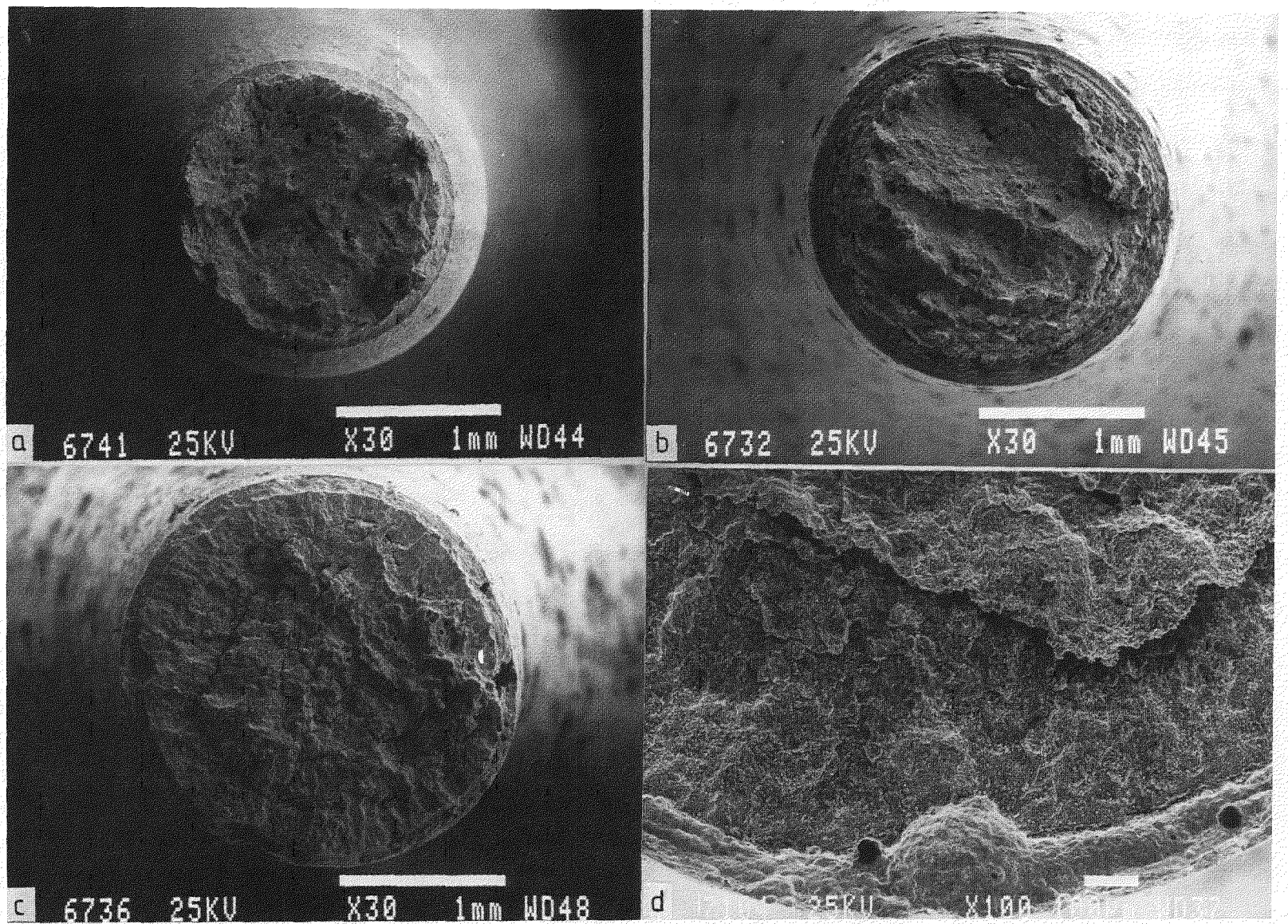

Fig. 11 Fracture surfaces of low-strain prefatigued A 516 Gr. 70 piping steel tested in deoxygenated PWR-Water at 288°C: (a) free corrosion potential (E = -830 mV(SHE)), (b) controlled potential at -1500 mV(SHE), (c) and (d) controlled potential at 0 mV(SHE).

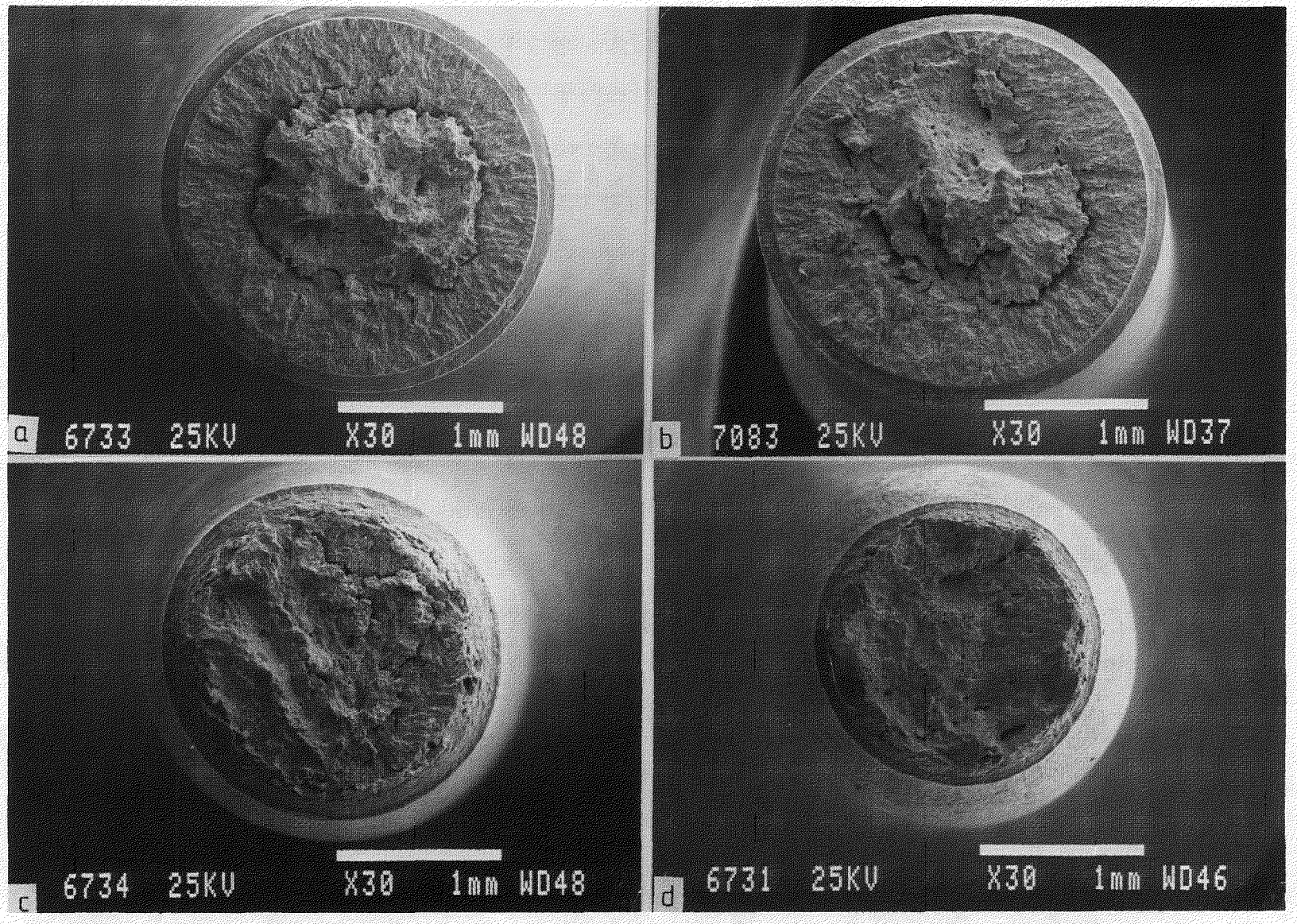

Fig. 12 Fracture surfaces of four low-strain prefatigued A 516 Gr. 70 piping steel notched specimens tested in MnS-saturated deoxygenated PWR-Water at 288°C: (a) E = -510 mV(SHE), (b) E = -580 mV(SHE), (c) E = -660 mV(SHE), and (d) E = -680 mV (SHE).

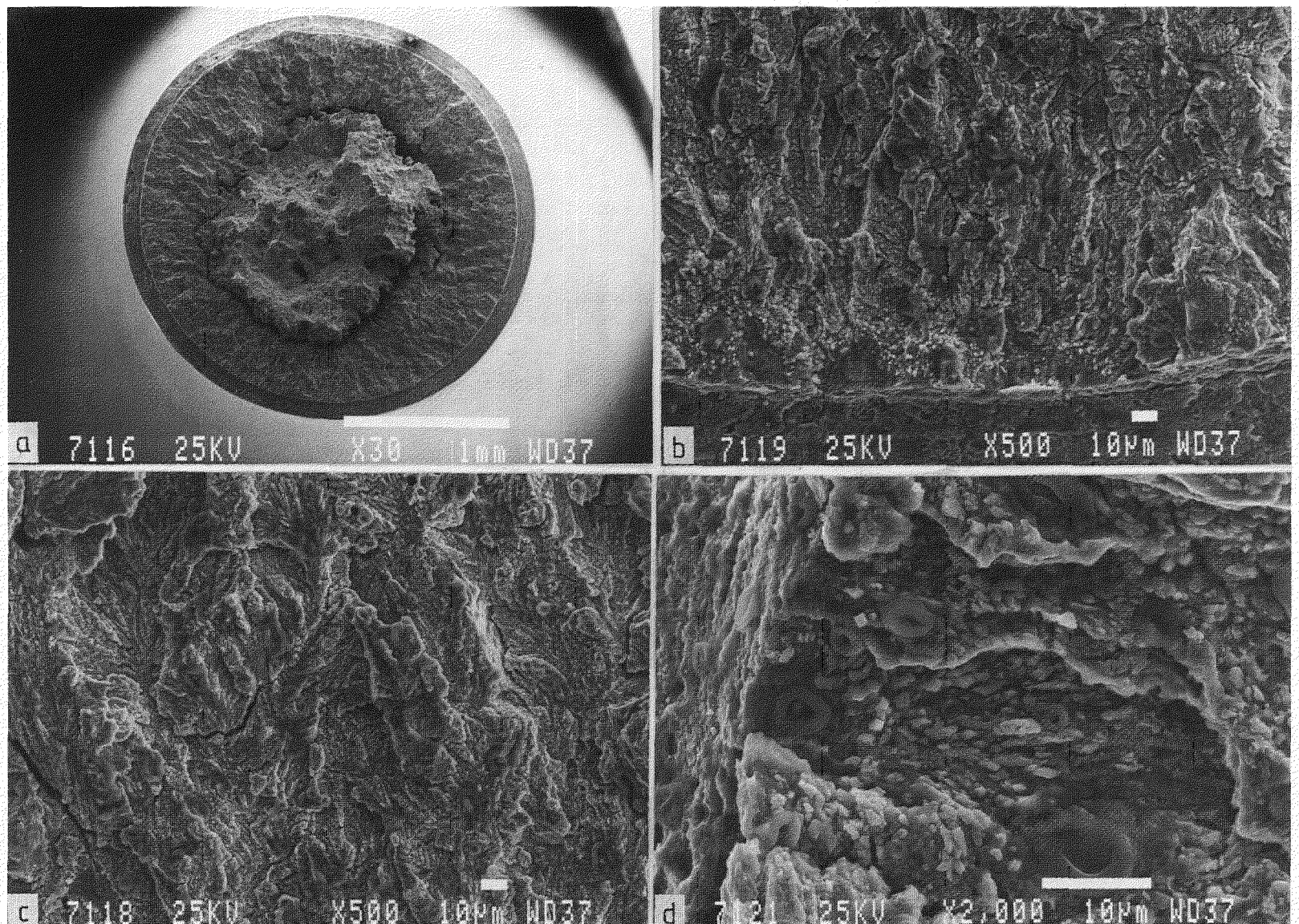

Fig. 13 Fracture surface of low-strain prefatigued A 516 Gr. 70 piping steel notched specimen tested in MnS-saturated deoxygenated PWR-Water at 288°C (E = -510 mV (SHE).

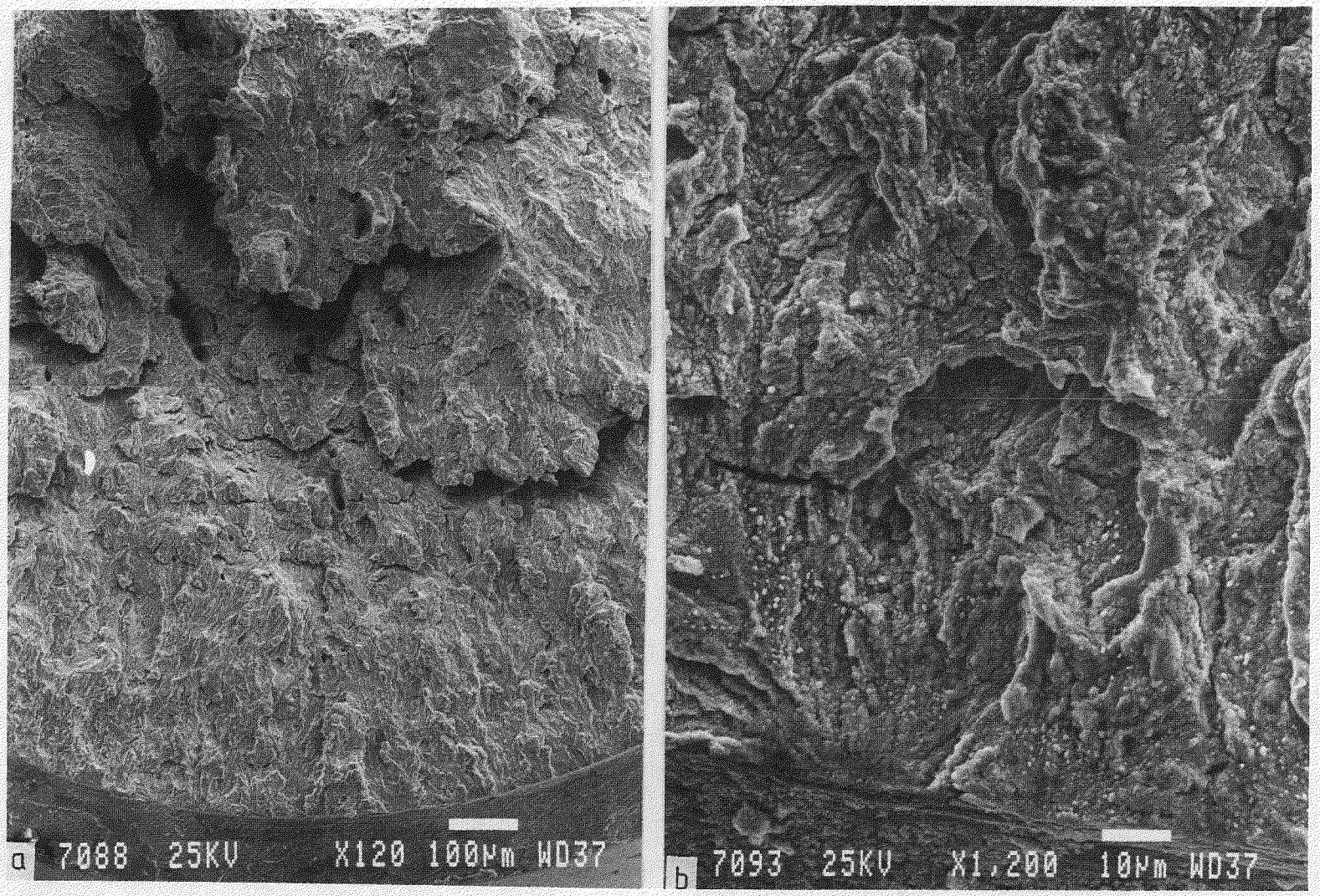

Fig. 14 Details of the fracture surface of low-strain prefatigued A 516 Gr. 70 piping steel specimen tested in MnS-saturated deoxygenated PWR-Water at 288°C, E = -580 mV(SHE).

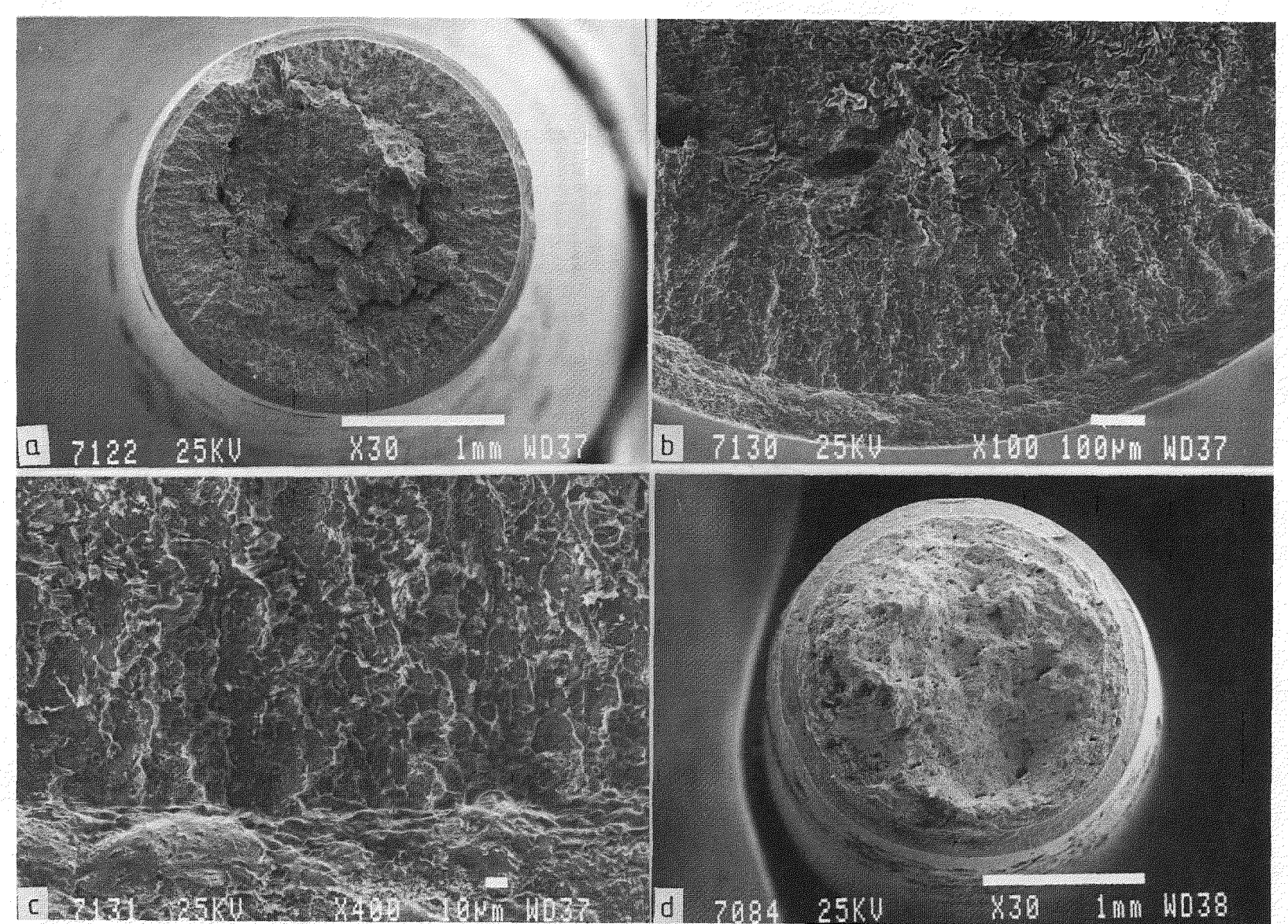

Fig. 15 Fracture surfaces of low-strain prefatigued A 516 Gr. 70 steel notched specimens tested under external potential control in MnS-saturated deoxygenated PWR-Water at 288°C: (a) through (c) 0 mV(SHE), and (d) -1500 mV(SHE).

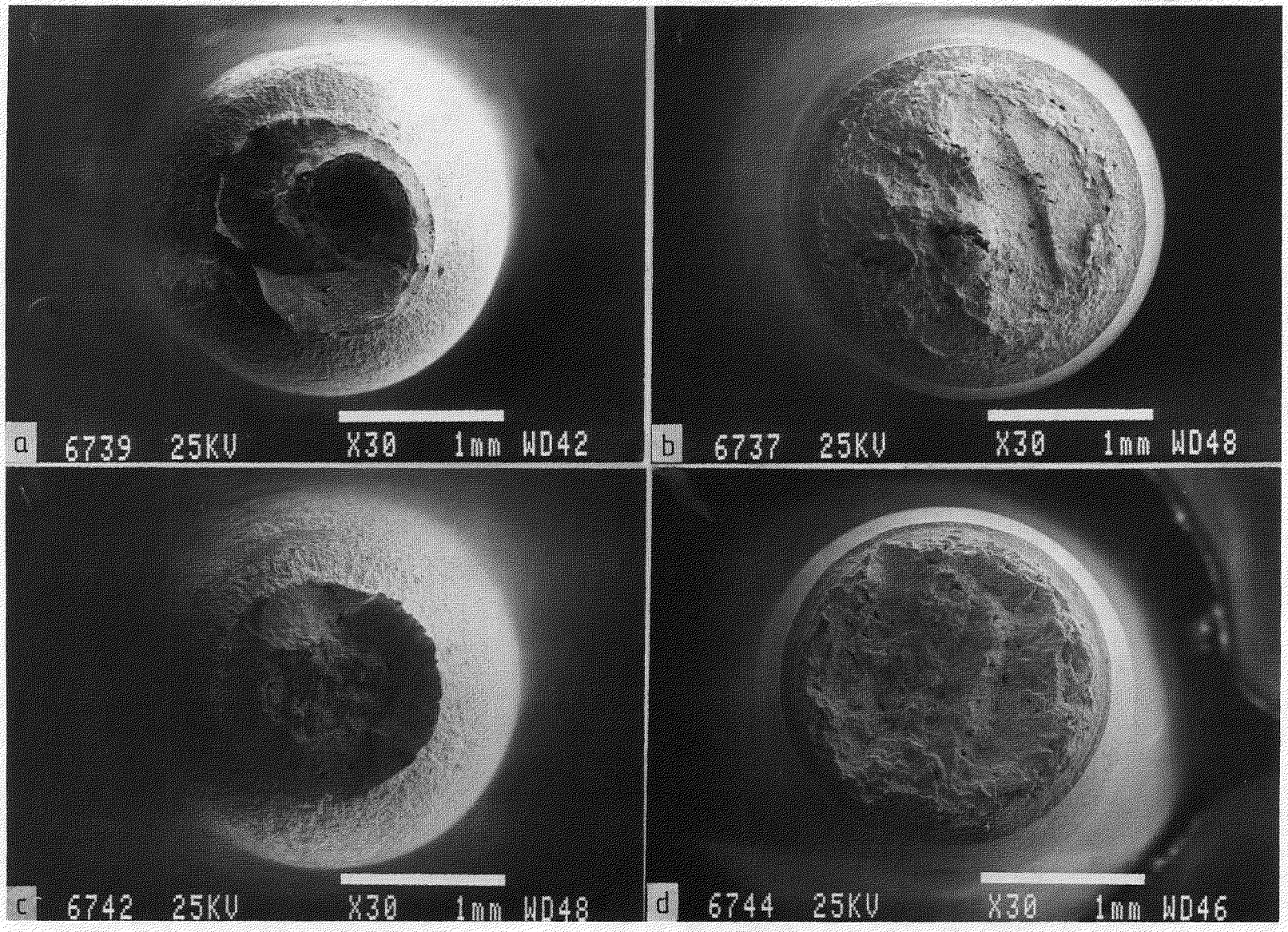

Fig. 16 Fracture surfaces of high-strain prefatigued A 516 Gr. 70 piping steel smooth and notched specimens: (a) and (b) in helium at 288°C (c) and (d) in deoxygenated PWR-Water at 288°C.

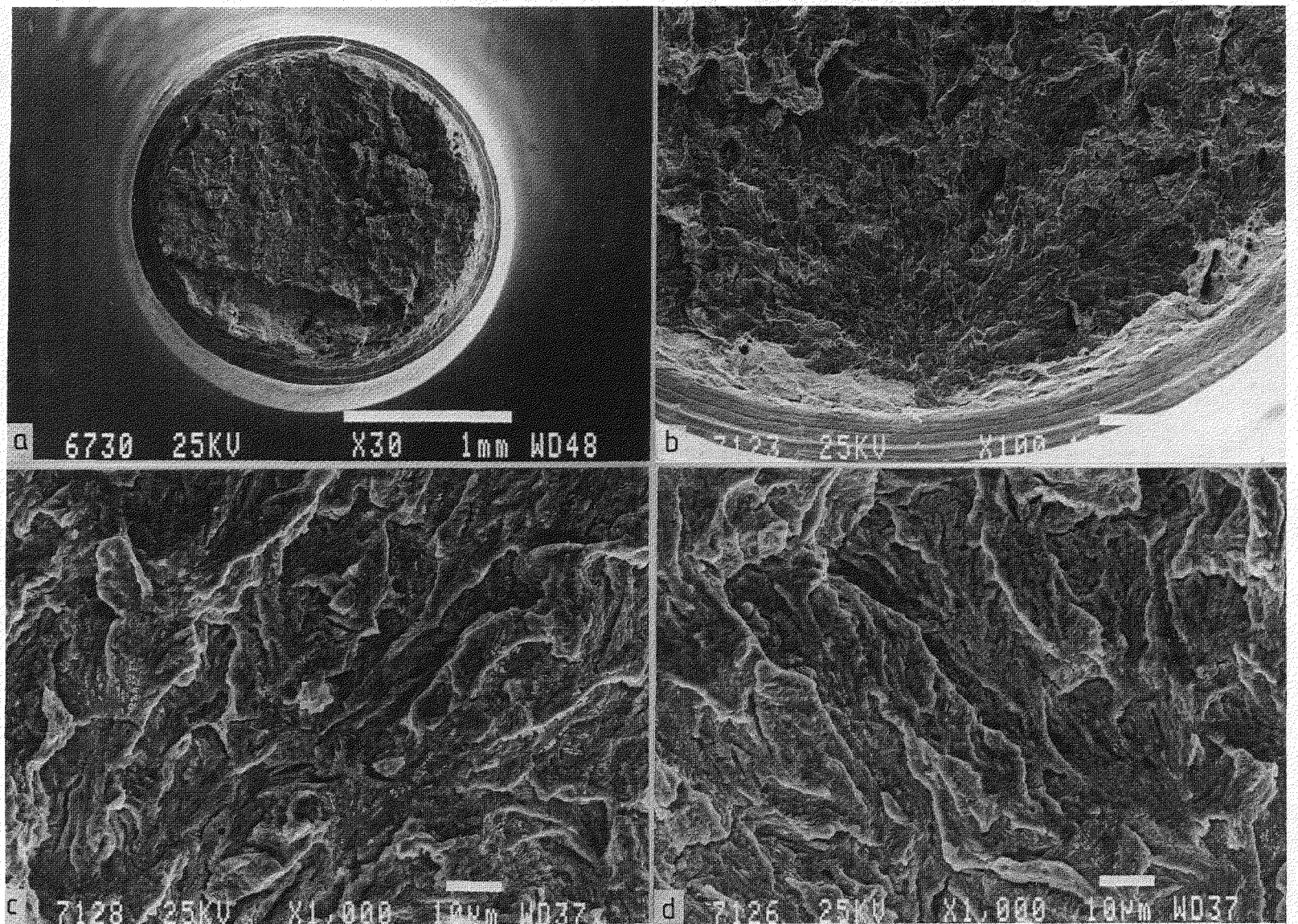

Fig. 17 Fracture surface of high-strain prefatigued A 516 Gr. 70 piping steel notched specimen tested in MnS-saturated deoxygenated PWR-Water at 288°C (E = -570 mV(SHE)).

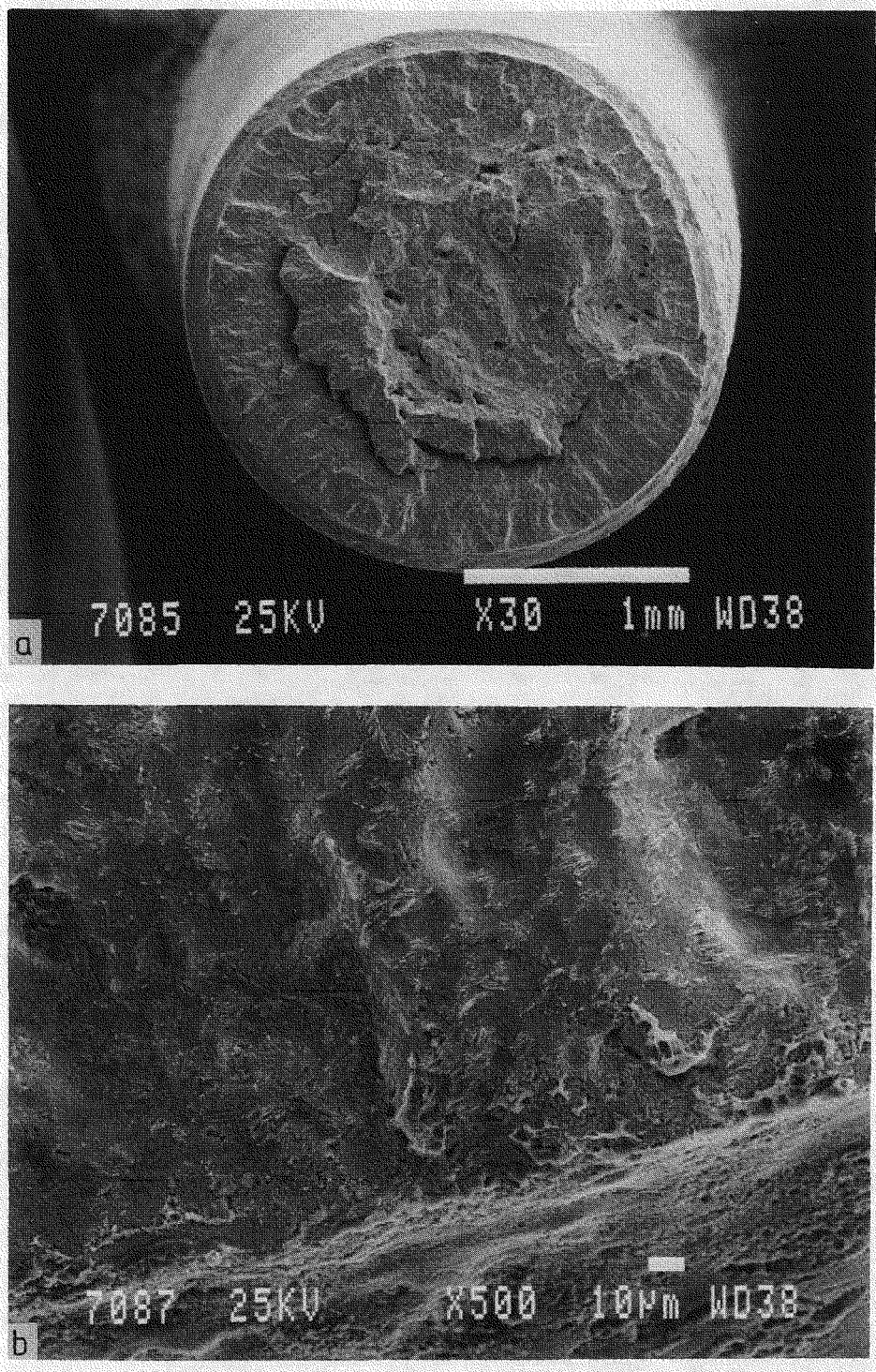

Fig. 18 Fracture surface of high-strain prefatigued A 516 Gr. 70 piping steel notched specimen tested in MnS-saturated deoxygenated PWR-Water at 288°C under external potential control at 0 mV(SHE).

under external anodic polarization to 0.0 mV(SHE), Fig. 18. At the high potential the specimen was markedly attacked by the environment, Fig. 18b.

Stress corrosion occurred either in MnS-saturated PWR-water, or in pure PWR-water when specimens were anodically polarized to 0.0 mV(SHE). In Table 4 SCC can be seen as a short elongation to fracture (A) and especially low values of reduction of area (Z) and equivalent plastic strain at fracture. The fracture surfaces of most of the specimens were shown in Figs. 8 to 18.

The observed SCC crack growth rates are summarized in Table 5. It can be seen that at lower potentials cracking occurs only in MnS-saturated conditions, where corrosion potential is between -510 to -650 mV(SHE); lowering corrosion potential reduces the crack growth rate. When the specimen is polarized to 0.0 mV(SHE), the crack growth rate is about the same in pure PWR-conditions, as compared to MnS-saturated PWR-water. Based on these results there are no marked differences between unstrained and prefatigued materials.

The crack growth rate values in Table 5 are based on the premise that the initiation of cracks takes place when the yield stress, determined from the load-time curve, is exceeded. If initiation takes place later, the crack growth rate is then correspondingly higher. These crack growth rates are about the same as the time-based crack growth rates generally determined for pressure vessel steels from tests with large fracture mechanics specimens in reactor water; typically the maximum crack growth rate from both cyclic and SSRT-tests is 7×10^{-8} m/s (Ref. 37). In this case the supply of needed sulfur comes from the randomly distributed MnS-inclusions of the steels. It can now be stated that the above mentioned value of crack growth rate is a reliable estimate for worst case situations for environmentally enhanced, time-based crack growth of carbon and low alloy steels. Also it can be observed that the prefatigued materials do not show higher crack growth rates than the as-received virgin material. This also clarifies the similar behavior of environmentally enhanced crack growth rates in cyclic loading, where the crack tip material can be considered to correspond the material used in this study, as compared to SCC tests.

Another important factor was that the average external corrosion potential in MnS-saturated PWR-water experiments was -590 mV(SHE) and it generally was -750 to -850 mV(SHE) in the pure PWR-water experiments. On the basis of Pourbaix diagrams these higher potential values are in the areas of H_2S, FeS_2, and FeS which are stable corrosion products in this case. It can be argued that in corrosion fatigue testing of steels in typical reactor water, the crack tip environment which produces the high crack growth rate is similar to that created in this study, in other words, the MnS-saturated PWR-water. This means that in BWR-water, where the external potential is high, the crack-tip potential is lower than the external corrosion potential and in PWR-water where the external potential is low the crack-tip potential can be higher near dissolving MnS inclusions.

Table 5 The SCC crack growth rates for notched A 516 Gr. 70 piping steel specimens, when the crack initiation stage is estimated to be while passing the yield point.

Material	Condition	Crack growth rate, m/s
As-received	PWR + MnS, E = -650 mV(SHE)	2.1×10^{-8}
Low strain prefatigue	PWR + MnS, E = -510 mV(SHE)	2.5×10^{-8}
Low strain prefatigue	PWR + MnS, E = -580 mV(SHE)	2.7×10^{-8}
Low strain prefatigue	PWR + MnS, E = -660 mV(SHE)	2.8×10^{-9}
Low strain prefatigue	PWR + MnS, E (applied) = 0.0 mV(SHE)	3.3×10^{-8}
Low strain prefatigue	PWR-Water, E (applied) = 0.0 mV(SHE)	2.5×10^{-8}
High strain prefatigue	PWR + MnS, E = -570 mV(SHE)	1.2×10^{-8}
High strain prefatigue	PWR + MnS, E (applied) = 0.0 mV(SHE)	2.5×10^{-8}

4.4 Residual Hydrogen Contents

In order to evaluate the role of absorbed hydrogen in environment-sensitive cracking of these SSRT specimens some specimens were selected for residual hydrogen analysis. Table 6 shows the results obtained from A 516 Gr. 70 piping steel specimens evaluated more than half a year following completion of actual SSRT-testing. The reference hydrogen content was 2.2 ppm, and most of the specimens showed increased hydrogen contents after exposure to environments. Some comparisons between gage section and the thicker section of the specimen which had been exposed to the same autoclave environment showed that the gage length was showing higher hydrogen contents. No clear differences between SSRT specimens of unstrained material and prefatigued materials could be seen. A before and after effect was observed when oxide removal was applied to ARSN-10 specimen, but it could not be adequately explained. Many of the gage length specimens had experienced oxide removal a significant time before hydrogen content measurement, in order to prepare the fracture surface for SEM examination.

Table 6 Residual Hydrogen contents of the A 516 Gr. 70 specimens after SSRT-testing

Specimen	Corrosion Potential (mV)	Location	H-content (ppm)
Reference Material (Unexposed)	----	----	2.2
PFSPN-6, PWR-water	----	gage length	4.1; 2.2
PFSPN-6, PWR-water	----	thick section	2.1
PFSN-12, PWR-water	0	gage length	3.5; 2.6
PFSN-12, PWR-water	0	thick section	2.1
PFSN-15, PWR + MnS	-510	gage length	1.3; 1.2
PFSN-15, PWR + MnS	-510	thick section	1.8
PFSN-17, PWR-water	-1500	gage length	2.9; 3.5
PFSN-17, PWR-water	-1500	thick section	2.0
ARSN-10, PWR + MnS	-650	thick section with oxide	5.0; 3.2
ARSN-10, PWR + MnS	-650	thick section after oxide removal	0.6; 0.4
ARSN-10, PWR + MnS	-650	gage length	4.9
PFSN-13, PWR + MnS	-660	gage length	3.5

5. DISCUSSION

Ahead of the corrosion fatigue crack-tip, the most important mechanism for the accomodation of large strains is the formation of the dislocation cell structure. Just ahead of the crack-tip at high strains an equiaxed cell size is formed, where cell walls are impenetrable by dislocations due to high misorientation. Similar metallurgical conditions have been simulated in this study in order to understand the micromechanisms of environmentally enhanced crack growth and in order to obtain maximum possible crack growth rate values. SSRT-tests with as-received materials as well as prefatigued materials showed that prefatigue affected only the yield and ultimate tensile stress values, increasing them due to cyclic hardening of the material. In tests where SCC did not occur, elongation to fracture and reduction of area were even higher in highly prefatigued material as compared to as-received material.

Liaw and Landes (Refs. 38 and 39) have studied the effects of previous load histories on fracture toughness properties of 4340 steel and AISI 316 stainless steel. They observed that the effects of cyclic prestrain on fracture toughness could be related to cyclic softening characteristies of the 4340 steel and cyclic hardening of AISI 316 steel, respectively. Cyclic softening increased the fracture toughness of 4340 steel and decreased that of AISI 316 steel, i.e., the toughness behavior could be rationalized by material strength levels. The results of this study indicate that in case of A 516 Gr. 70 steel, which showed slight cyclic hardening, the mechanical properties are improved in SSRT-tests.

When SCC was taking place in MnS-contaminated PWR-water or in pure as well as MnS-contaminated PWR-water under external polarization to 0.0 mV(SHE), the effect of microstructure (as-received or prefatigued) did not seem to play any major role as far as the effects on the maximum crack growth rates are considered. Also the fracture surfaces were identical and no signs of prefatigue dislocation cell structure can be discerned from the SCC fracture surfaces. This explains also why the environment-enhanced brittle-like corrosion fatigue fracture surface is similar to SCC fracture surface (Figs. 15 and 17) obtained e.g., in conventional SSRT-tests. Therefore, one can expect that there must be some kind of mechanism leading to breakdown of the dislocation cell structure formed ahead of the advancing corrosion fatigue crack-tip which then leads to similar deformation mechanisms which can take place in as-received material in a conventional SSRT-type of test.

When the corrosion fatigue crack-tip conditions were simulated by MnS-addition to the test environment, the significant effect was an increase of the corrosion potential from a range of -750 to -850 mV(SHE) to a range of -510 to -650 mV(SHE), i.e., into the area in the potential-pH diagrams where H_2S and FeS_2/FeS are stable phases. This increase in potential may be explained by the acidification of the environment if the corrosion potential follows the hydrogen line in the diagram. Only one specimen exposed to MnS-saturated water did not show cracking in these tests and in this case for some unknown reason the corrosion potential was an unexpectedly low -680 mV(SHE). Another

specimen having a corrosion potential of -660 mV(SHE) exhibited minor cracking compared to cracking in other specimens at higher free corrosion potentials. Therefore even in these MnS-contaminated conditions there may be a corrosion potential threshold for environment-sensitive cracking to occur. When specimens were cathodically polarized to -1500 mV(SHE) only reduced ductility with ductile cracking could be observed and MnS did not seem to show any effect. After polarizing to 0.0 mV(SHE) all the specimens cracked at about the same rate and again MnS-contamination did not play any major role, as compared with pure PWR-water. It may be concluded that MnS-contamination in PWR-conditions reduces the threshold potential for environment-sensitive cracking, as compared to pure PWR-water (~ -200 mV(SHE)). The lowest corrosion potential exhibiting cracking in MnS-contaminated PWR-water was -660 mV(SHE), whereas at -680 mV(SHE) no cracking was observed in this study. Mechanistically it is still unclear if a threshold potential for cracking really exists and which are the controlling parameters for that phenomenon.

A first attempt was made to measure the residual hydrogen contents of the SSRT-test specimens, in order to understand if the conditions causing cracking also enhance markedly hydrogen uptake into test specimens. Increased residual hydrogen contents were clearly observed, but since the measurements were performed more than half a year after actual testing, there has been plenty of time for hydrogen to diffuse out of the specimens. In the future specimens should be transferred directly from the autoclave into a hydrogen analysis instrument in order to obtain more reliable values for absorbed hydrogen.

Mechanistically, cracking was thought to occur by hydrogen-induced mechanism, where critical parameters are hydrogen-enhanced plasticity and strain localization at shear bands at the notch root, which causes the breakdown of the dislocation cell structure in pre-fatigued materials. The fact of similar crack growth rates in both as-received and pre-fatigued materials is not in favor of a slip dissolution-type mechanism, because deformation processes in as-received and cyclically stabilized materials are very different.

By using this technique we expect that the measured crack growth values are the maximum values for this material environment system. The major unknown factor in determining these growth rate values is the initiation of cracking which may occur after the yield point even in notched specimens. Such a revaluation would change the results obtained only slightly. This kind of testing could be used in the future, for instance for measuring the activation energy for cracking, the dependence of crack growth on applied potential, and for hydrogen uptake in crack-tip conditions.

6. CONCLUSIONS

The following conclusions may be derived from this study:

- In conditions where SCC did not occur, prefatigue clearly improved the mechanical properties of A 516 Gr. 70 piping steel.

- Environment-sensitive cracking occurred in MnS-saturated PWR-water conditions and under anodic polarization to 0.0 mV(SHE) even in pure PWR-water.

- MnS raised the electrochemical potential of the steel to the range of -510 to -650 mV(SHE) in PWR primary water, i.e., in the stability areas of FeS_2, FeS and H_2S. This level of polarization is also expected to develop inside the cracks due to solubilizing MnS-inclusions.

- Crack growth rate was about the same in prefatigued materials, (i.e. ~ 2 to 3 x 10^{-8} m/s,) as in as-received material. The estimated crack growth rates are of the same order of magnitude as the highest measured values for fracture mechanics specimens of low alloy steels, ~ 7 x 10^{-8} m/s.

- Mechanistically, cracking was thought to occur by hydrogen-induced mechanism, where critical parameters are hydrogen-enhanced plasticity and strain localization at shear bands at the notch root, which causes the breakdown of the dislocation cell structure in prefatigued materials.

REFERENCES

1. M. O. Speidel and R. M. Magdowski, "Stress Corrosion Cracking and Corrosion Fatigue of Nuclear Reactor Pressure Vessel Steel," in SMiRT Post Conference Seminar No. 2, Session II, Davos, Switzerland, Aug. 24-25, 1987.

2. P. Hurst, D. A. Appleton, P. Banks, and A. S. Raffel, "Slow Strain Rate Tests on A 508-III and A533B Steels in Deionised and PWR Water at 563°K," Corrosion Science, Vol. 25, 1985, pp. 651-671.

3. J. Congleton and P. Hurst, "Slow Strain Rate Stress Corrosion Testing of RPV Steels in High Temperature Water," Proceedings of the Second International Atomic Energy Agency Specialists' Meeting on Subcritical Crack Growth, W. H. Cullen, Ed., USNRC Conference Proceeding NUREG/CP-0067, Vol. 1, 1986, pp. 439-463.

4. H. C. Cowen, P. Hurst, and G. J. Lloyd, "The ICCGR Inter-Laboratory Round Robin on Slow Strain Rate Stress Corrosion Testing of PWR Forging," Proceedings of the Second International Atomic Energy Agency Specialists' Meeting on Subcritical Crack Growth, W. H. Cullen, Ed., USNRC Conference Proceeding NUREG/CP-0067, Vol. 1, 1986, pp. 181-197.

5. P. Hurst, P. Banks, G. Pemberton, and A. S. Raffel, "Stress Corrosion Behaviour of A 533B and A 508-III Steels and Weldments in High Temperature Water Environments," Proceedings of the Second International Symposium on Environmental Degradation of Materials in Nuclear Power Systems -- Water Reactors, ANS, 1986, pp. 645-655.

6. M. E. Indig, J. E. Weber, and D. Weinstein, "Environmental Aspects of Carbon Steel Stress Corrosion in High Purity Water," Reviews in Coatings and Corrosion, Vol. 5(1-4), 1982, pp. 173-225.

7. S. Pednekar, T. Mizuno, Z. Szklarska-Smialowska, and D. D. MacDonald, "Stress Corrosion Cracking Behavior of Carbon Steel in High-Purity Water at 100 to 288°C," Corrosion/82, Houston, TX, Paper 244, 1982.

8. H. Choi, F. H. Beck, Z. Szklarska-Smialowska, and D. D. MacDonald, "Stress Corrosion Cracking of ASTM A 508 Cl.2 Steel in Oxygenated Water at Elevated Temperatures," Corrosion, Vol. 38, 1982, pp. 136-144.

9. E. Lenz, N. Wieling, G. Neubrech, "CERT-Data and Their Relevance for Corrosion Assessments of Cases," Proceedings of the Second International Atomic Energy Specialists' Meeting on Subcritical Crack Growth, W. H. Cullen, Ed., USNRC Conference Proceeding NUREG/CP-0067, Vol. 2, 1986, pp. 455-473.

10. J. Kuniya, I. Masaoka, R. Sasaki, H. Itoh, and T. Okazaki, "Stress Corrosion Cracking Susceptibility of Low Alloy Steels Used for Reactor Pressure Vessel Steels for Reactor Pressure Vessel in High Temperature Oxygenated Water," Trans. ASME Journal of Pressure Vessel Technology, Vol. 107, 1985, pp. 431-435.

11. K. Klemetti and H. Hanninen, "Effect of Electrochemical Potential on Stress Corrosion of Steel A 508 in BWR Environment," Proceedings of the Second International Symposium on Environmental Degradation of Materials in Nuclear Power Systems -- Water Reactors, NACE, Houston, TX 77084, 1987, pp. 70-76.

12. J. Congleton, T. Shoji, and R. N. Parkins, "The Stress Corrosion Cracking of Reactor Pressure Vessel Steel in High Temperature Water," Corrosion Science, Vol. 25, 1985, pp. 633-650.

13. J. Congleton and R. N. Parkins, "Stress Corrosion Cracking of Steel in High Temperature Water," Corrosion 87, San Francisco, CA, Paper No. 105, 1987.

14. J. Congleton and T. Shoji, "Slow Strain Rate Testing of RPV Steels in High Temperature Water," Structural Mechanics in Reactor Technology, Volume F: LWR Pressure Components, F. H. Wittmann, Ed., A. A. Balkema, Boston, MA, 1987, pp. 265-270

15. T. Shoji and H. Takahashi, "Factors Affecting Critical Cracking Potential of RPV in High Temperature Waters," presented at International Cyclic Crack Growth Rate Meeting, Aug. 11-14, 1987, Erlangen/Stuttgart, FRG, 1987.

16. H. Hanninen, K. Torronen, K. Kemppainen, and S. Salonen, "On the Mechanics of Environmental Sensitive Cyclic Crack Growth of Nuclear Reactor Pressure Vessel Steels," Corrosion Science, Vol. 23(6), 1983, pp. 663-679.

17. K. Klemetti, H. Hanninen, K. Torronen, M. Kemppainen, and M. Pessa, "On the Role of Inclusions in Environment Sensitive Cracking of Reactor Pressure Vessel Steels," Proceedings of the International Symposium on Environmental Degradation of Materials in Nuclear Power System -- Water Reactors, NACE, Houston, TX 77084, 1984, pp. 368-383.

18. F. P. Ford, D. F. Taylor, P. L. Andresen, and R. G. Ballinger, "Corrosion-Assisted Cracking of Stainless and Low-Alloy Steels in LWR Environments," Final Report, NP-5064M, Electric Power Research Institute, Palo Alto, CA, Feb. 1987.

19. H. Illi, E. Chanfreau, and H. Hanninen, "Application of Miniature Autoclaves in the Study of Crevice Chemistry at High Temperatures," Conference on Corrosion Chemistry Within Pits, Crevices, and Cracks, A. Turnbull, Ed., National Physical Laboratory, Teddington, 1987, pp. 645-651.

20. H. Hanninen, H. Illi, and M. Kemppainen, "Stress Corrosion Cracking of A 508 Steel in Saturated MnS-Solution," Proceedings NATO Advanced Research Workshop Chemistry and Physics of Fracture, R. M. Latanision, Ed., Martinus Nijhoff Publishers BV, Dordrecht, The Netherlands, 1987, pp. 646-651.

21. J. Congleton, "Experiments on the Effect of Applied Potential on the Susceptibility of A 508 and A 533B RPV Steels in PWR Water," presented at International Cyclic Crack Growth Rate Meeting, Aug. 11-14, 1987, Erlangen/Stuttgart, FRG, 1987.

22. W. A. Van Der Sluys and R. H. Emanuelson, "Enhancement of Fatigue Crack Growth Rates in Pressure Boundary Materials Due to Light-Water-Reactor-Environments," Third International Symposium on Environmental Degradation of Materials in Nuclear Power System -- Water Reactors, G.J. Theus and J.R. Weeks, Eds., TMS-AIME, Warrendale, PA, 1987, pp. 277-282.

23. G. Slama and P. Rabbe, "French Approach and Results in Cyclic Crack Growth," Proceedings of the 5th SMiRT Post-Conference Seminar, Applied Science Publishers, London, 1982, pp. 311-325.

24. W. H. Bamford, L. J. Ceschini, and R. J. Jacko, "Environmentally Assisted Crack Growth Studies," in Heavy Section Steel Technology Report for July-September 1983, USNRC Report NUREG/CR-3334, Vol. 3, Mar. 1984, pp. 97-114.

25. W. A. Van Der Sluys, "Corrosion Fatigue Characterization of Reactor Pressure Vessel Steel," Progress Report, October 1, 1982 to April 30, 1983, Project 1325-1, Electric Power Research Institute, Palo Alto, CA, July 1983.

26. W. H. Cullen, M. Kemppainen, H. Hanninen, and K. Torronen, "The Effects of Sulfur Chemistry and Flow Rate on Fatigue Crack Growth Rates in LWR Environments," USNRC Report NUREG/CR-4121, Feb. 1985.

27. H. Hanninen, M. Vulli, and W. H. Cullen, "Study of Corrosion Products on Fatigue Fracture Surfaces of Pressure Vessel Steels Tested in PWR Environments by Using X-Ray Photoelectron and Auger Electron Spectroscopies," Third International Symposium on Environmental Degradation of Materials in Nuclear Power System -- Water Reactors, G. J. Theus and J. R. Weeks, Eds., TMS-AIME, Warrendale, PA, pp. 289-299, 1987.

28. H. Hanninen, H. Illi, K. Torronen, and M. Vulli, "On the Electrochemical and Chemical Conditions in Corrosion Fatigue Cracks of Low Alloy Steels in High Temperature Water," Proceedings of the Second International Atomic Energy Agency Specialists' Meeting on Subcritical Crack Growth, W. H. Cullen, Ed., USNRC Conference Proceeding NUREG/CP-0067, Vol. 2, 1986, pp. 179-199.

29. H. Hanninen, K. Torronen, and W. H. Cullen, "Comparison of Proposed Cyclic Crack Growth Mechanisms of Low Alloy Steels in LWR Environments," Proceedings of the Second International Atomic Energy Agency Specialists' Meeting on Subcritical Crack Growth, W. H. Cullen, Ed., USNRC Conference Proceeding NUREG/CP-0067, Vol. 2, 1986, pp. 73-97.

30. F. P. Ford, "Overview of Collaborative Research into the Mechanisms of Environmentally Controlled Cracking in the Low Alloy Pressure Vessel Steel/Water System," Proceedings of the Second International Atomic Energy Agency Specialists' Meeting on Subcritical Crack Growth, W. H. Cullen, Ed., USNRC Conference Proceeding NUREG/CP-0067, Vol. 2, 1986, pp. 3-72.

31. W. H. Cullen, G. Gabetta, and H. Hanninen, "A Review of the Models and Mechanisms for Environmentally-Assisted Crack Growth of Pressure Vessel and Piping Steels in PWR Environments," USNRC Report NUREG/CR-4422, Dec. 1985.

32. J. D. Atkinson and J. E. Forrest, "The Role of MnS Inclusions in the Development of Environmentally Assisted Cracking of Nuclear Reactor Pressure Vessel Steels," Proceedings of the Second International Atomic Energy Agency Specialists' Meeting on Subcritical Crack Growth, W. H. Cullen, Ed., USNRC Conference Proceeding NUREG/CP-0067, Vol. 2, 1986, pp. 153-178.

33. P. Combrade, M. Foucault, and G. Slama, "About the Crack Tip Environment Chemistry in Pressure Vessel Steel Exposed to Primary PWR Coolant," Proceedings of the Second International Atomic Energy Agency Specialists' Meeting on Subcritical Crack Growth, W. H. Cullen, Ed., USNRC Conference Proceeding NUREG/CP-0067, Vol. 2, 1986, pp. 201-218.

34. F. P. Ford and P. Combrade, "Electrochemical Reaction Rates on Bare Surfaces and Their Use in a Crack Prediction Model for the Low-Alloy Steel/Water System," Proceedings of the Second International Atomic Energy Agency Specialists' Meeting on Subcritical Crack Growth, W. H. Cullen, Ed., USNRC Conference Proceeding NUREG/CP-0067, Vol. 2, 1986, pp. 231-268.

35. F. P. Ford, "Status of Research on Environmentally-Assisted Cracking in LWR Pressure-Vessel Steels," Performance and Evaluation of Light Water Reactor Pressure Vessels, PVP-119, American Society of Mechanical Engineering, New York, NY, 1987, pp. 43-62.

36. R. E. Peterson, Stress Concentration Factors, John Wiley & Sons, New York, 1953.

37. M. O. Speidel, "Stress Corrosion Cracking Of Nuclear Pressure Vessel Steel" Proceedings of the Second International Atomic Energy Agency Specialists' Meeting on Subcritical Crack Growth, W. H. Cullen, Ed., USNRC Conference Proceeding NUREG/CP-0067, Vol. 1, 1985, pp. 465-476.

38. P. K. Liaw and J. D. Landes, "Influence of Prestrain History on Fracture Toughness Properties of Steels," Metallurgical Transactions, Volume 17A, March 1986, pp. 473-489.

39. P. K. Liaw and J. D. Landes, "Effects of Monotonic and Cyclic Prestrain on Fracture Toughness: A Summary," Fracture Mechanics: Eighteenth Symposium, ASTM STP 945. D. T. Read and R. P. Reed, Eds., American Society for Testing and Materials, Philadelphia, 1988, pp. 622-646.